Fast and exact synthesis of some operator scaling Gaussian random fields

Hermine Biermé, Céline Lacaux

FAST AND EXACT SYNTHESIS OF SOME OPERATOR SCALING GAUSSIAN RANDOM FIELDS

HERMINE BIERMÉ AND CÉLINE LACAUX

Abstract. Operator scaling Gaussian random fields, as anisotropic generalizations of self-similar fields, know an increasing interest for theoretical studies in the literature. However, up to now, they were only defined through stochastic integrals, without explicit covariance functions. In this paper we exhibit explicit covariance functions, as anisotropic generalizations of fractional Brownian fields ones, and define corresponding Operator scaling Gaussian random fields. This allows us to propose a fast and exact method of simulation based on the circulant embedding matrix method, following ideas of Stein [34] for fractional Brownian surfaces syntheses. This is a first piece of work to popularize these models in anisotropic spatial data modeling.

Keywords: Operator scaling, Self-similarity, Gaussian field, Fractional Brownian fields, Anisotropy, Covariance, Simulation

2010 Mathematics Subject Classification. Primary: 60G60, 60G15, 60-04, ; Secondary: 60G22 60G17

1. Introduction

In spatial or image analysis, the correlation dependency is of crucial interest. Scale invariance properties are also usually investigated, in particular for rough data, where fractal analysis might help for classification (see [26] for a good review in medical imaging). Actually, numerous natural phenomena have been shown to be self-similar. Let us recall that a scalar-valued random field $(X(x))_{x\in\mathbb{R}^d}$ is said to be *H-self-similar* with $H>0$ if

$$\{X(cx); x\in\mathbb{R}^d\} \overset{(fdd)}{=} \{c^H X(x); x\in\mathbb{R}^d\} \tag{1}$$

for every $c>0$, where $\overset{(fdd)}{=}$ means equality of finite dimensional distributions. For instance, self-similar random fields can model persistent phenomena in internet traffic, hydrology, geophysics or financial markets, e.g. [24, 1, 31, 35]. An additional invariance assumption often required is the stationary property. A random field $(X(x))_{x\in\mathbb{R}^d}$ is called stationary if its law is invariant under translation meaning that for all $h\in\mathbb{R}^d$,

$$\{X(x+h); x\in\mathbb{R}^d\} \overset{(fdd)}{=} \{X(x); x\in\mathbb{R}^d\}.$$

This property is useful for homogeneous modeling. However this is not compatible with the self-similarity property. Hence it is usually relaxed using the assumption of *stationary increments* property, also named as *intrinsically stationary* property. This means that for all lag $h\in\mathbb{R}^d$, the increment process with lag h defined by

$$\forall x\in\mathbb{R}^d,\ \Delta_h X(x) = X(x+h)-X(x), \tag{2}$$

is a stationary random field. Note that any stationary random field has stationary increments but the converse is false. A very important and common class of fields are given by centered Gaussian random fields. In this setting, according to stationary increments property (2), assuming that X is centered with $X(0)=0$ almost surely, the distribution of the field is entirely characterized by its covariance function given by

$$\forall x,y\in\mathbb{R}^d,\ \ \mathrm{Cov}(X(x),X(y)) = v_{_X}(y)+v_{_X}(x)-v_{_X}(x-y), \tag{3}$$

Date: March 9, 2017.

This work has been supported by the GDR CNRS 3477 and the GDR CNRS 3475.

where $v_{_X}$ is the so-called *semi-variogram* of X defined by

$$\forall h \in \mathbb{R}^d,\ v_{_X}(h) = \frac{1}{2}\mathbb{E}\left((X(x+h) - X(x))^2\right). \tag{4}$$

Self-similarity property (1) implies now that $v_{_X}(ch) = c^{2H} v_{_X}(h)$, for all $h \in \mathbb{R}^d$ and $c > 0$. The most famous example of self-similar Gaussian random field with stationary increments is given by the fractional Brownian field B_H (fBf), where $H \in (0,1)$ is the so-called Hurst parameter. It is an isotropic generalization of the famous one-dimensional fractional Brownian motion, implicitly introduced in [23] and defined in [27], obtained replacing the absolute value $|\cdot|$ by the Euclidean norm $\|\cdot\|$ in the semi-variogram:

$$\forall x \in \mathbb{R}^d,\ \ v_{_{B_H}}(x) = \|x\|^{2H}. \tag{5}$$

Let us quote here that the standard fractional Brownian field with Hurst index H is usually defined with $v_{_{B_H}}/2$ as semi-variogram and corresponds to $B_H/\sqrt{2}$ with our convention. However, the choice of the Euclidean norm implies that the fractional Brownian field is isotropic. This is very restrictive for spatial data where anisotropy may be an important feature to take into account. Hence several anisotropic generalizations have been proposed. Most of them rely on the introduction of a *topothesy* function taking into account the influence of the direction in the semi-variogram (see [17]). Semi-variograms are usually obtained through integral formula (see [2] for instance) except for marginal cases (see Proposition 2.1 of [11]) and self-similarity does not vary according to directions. In order to exhibit this kind of anisotropy, observed for instance in geoscience [6, 13] or medical imaging [7], operator scaling property has been introduced as an anisotropic generalization of self-similarity property. More precisely, a scalar-valued random field $(X(x))_{x\in\mathbb{R}^d}$ is called *operator scaling* for E and $H > 0$ if for every $c > 0$

$$\{X(c^E x); x \in \mathbb{R}^d\} \overset{(fdd)}{=} \{c^H X(x); x \in \mathbb{R}^d\}, \tag{6}$$

where E is a real $d\times d$ matrix whose eigenvalues have positive real parts and as usual $c^E = \exp(E\log c)$ with $\exp(A) = \sum_{k=0}^{\infty} \frac{A^k}{k!}$ the matrix exponential. In particular for $E = \mathrm{diag}(\lambda_1, \ldots, \lambda_d)$, since $c^E = \mathrm{diag}(c^{\lambda}_1, \ldots, c^{\lambda}_d)$, this rewrites as

$$\{X(c^{\lambda_1}x_1, \ldots, c^{\lambda_d}x_d); x = (x_1, \ldots, x_d) \in \mathbb{R}^d\} \overset{(fdd)}{=} \{c^H X(x_1, \ldots, x_d); x \in \mathbb{R}^d\},$$

so that $\{X(te_j); t \in \mathbb{R}\}$ is H/λ_j self-similar, for any canonical direction e_j. Let us quote that when X is operator scaling for E and $H > 0$, it is also for E/H and 1 and (E, H) is not uniquely defined. We refer to [18] who characterized the possible set of exponents in the vectorial-valued framework of operator self-similar random fields. Note also that an H-self-similar field is also an operator scaling field for the matrix $E = I_d$, where I_d is the identity matrix of size $d \times d$. Now, for X a centered Gaussian field with stationary increments and semi-variogram $v_{_X}$ defined by (4), operator scaling property implies that the function $\tau_{_E} := v_{_X}^{1/2H} : \mathbb{R}^d \to \mathbb{R}^+$ is an E-homogeneous function in the sense of Definition 2.6 of [10] ie, for all $c > 0$

$$\forall x \in \mathbb{R}^d,\ \ \tau_{_E}(c^E x) = c\tau_{_E}(x).$$

Operator scaling Gaussian and α-stable random fields with stationary increments have been constructed in [10], using classical harmonizable or moving average representation under the assumption that $H \in (0, \min_{1\le j\le d} \lambda_j)$ where $\{\lambda_j; 1 \le j \le d\}$ are the positive real parts of the eigenvalues of the matrix E (see Section 2). Therefore, using harmonizable representation, approximate simulations methods known as spectral methods [29, 33] can be used. Based on a discretization of the spectral density used in the kernel of the stochastic integral, these methods induce periodization effects which allow the use of Fast Fourier Transform to get a very few computational cost. However they can not be exact and error bounds are not computed in general. When explicit covariance functions are known, exact methods of simulation for Gaussian random fields are usually based on the diagonalization of their covariance matrix [12, 14]. However, stochastic integral representations only allow to get integral formula for semi-variograms and no explicit semi-variograms for general E-operator scaling Gaussian random fields were known up to now.

In this paper, we define explicit semi-variograms for operator scaling Gaussian random fields. In particular, in Theorem 1, we prove that the function defined by

$$\forall x \in \mathbb{R}^d, v_{_X}(x) = \tau_{_E}(x)^{2H}, \text{ with } \tau_{_E}(x) = \left(\sum_{i=1}^{d} |\langle x, \theta_i \rangle|^{2a_i} \right)^{1/2}, \tag{7}$$

is the semi-variogram function of a Gaussian operator scaling random field for $0 < H \leq 1$ and E a diagonalizable matrix satisfying $E^t\theta_i = a_i^{-1}\theta_i$, with $a_i \in (0, 1]$ for $1 \leq i \leq d$ and E^t the transpose matrix of E. Here and in the sequel $\langle \cdot, \cdot \rangle$ denotes the Euclidean scalar product such that $v_{_{B_H}}$ is obtained for $E = I_d$. Let us also quote that the case $H = 1$ corresponds to the case of independence between eigenvectors directions. Actually, it is clear that the centered Gaussian random field $\left(\sum_{i=1}^{d} B_{a_i}^{(i)}(\langle x, \theta_i \rangle) \right)_{x \in \mathbb{R}^d}$, where $(B_{a_i}^{(i)})_{1 \leq i \leq d}$ are d independent fractional Brownian motions on $\mathbb{R}$ with respective semi-variograms given by (5), admits $\tau_{_E}^2$ for semi-variogram.

It follows that covariance matrix may now be computed but the computational cost for diagonalization is prohibitive, especially for dimension $d \geq 2$. In dimension $d = 1$ and $d = 2$, fast and exact simulation of stationary Gaussian random fields may be obtained on equispaced grid using circulant embedding matrix techniques developped in [19, 36]. They rely on the Toeplitz structure of covariance matrices and are exact as soon as a periodic representation may be found, with a circulant covariance matrix diagonalized by discrete Fourier transform. These ideas have been generalized for the exact simulation of fractional Brownian fields in [34]. Since fractional Brownian fields are not stationary, nor periodic, the main idea of Stein [34] is to consider a locally stationary representation of such fields. We follow this point of view in this paper. It consists in finding a stationary covariance function with compact support whose semi-variogram is close enough from the target one in a given window. Compact support ensures that its periodization remains a covariance function. Hence the circulant embedding matrix method may apply to simulate equispaced point of the associated stationary Gaussian random field.

This paper is organized as follows. Section 2 recalls some background on operator scaling Gaussian random fields and proposes a class of such fields with an explicit known semi-variogram. Then Section 3 presents the method of simulation, based on the simulation of a periodic stationary random field. The last section is devoted to a numerical study of the proposed method. Algorithms of simulation are postponed to Appendix.

2. Operator Scaling Gaussian Random fields

Explicit constructions of operator scaling Gaussian random fields were firstly given in [10]. Let E be a fixed $d \times d$ matrix such that $\{\lambda_j; 1 \leq j \leq d\}$ denote the positive real parts of its eigenvalues and $q = \mathrm{tr}(E)$. Choosing W a complex Gaussian random measure with Lebesgue control measure (see [31] p.281 for details on such measures), according to Theorem 4.1 and Corollary 4.2 of [10], when $\psi : \mathbb{R}^d \to [0, \infty)$ is a continuous, E^t-homogeneous function such that $\psi(x) \neq 0$ for $x \neq 0$, the harmonizable Gaussian random field

$$X_\psi(x) = \Re \int_{\mathbb{R}^d} \left(e^{i\langle x, \xi \rangle} - 1 \right) \psi(\xi)^{-H-q/2} \, W(d\xi) \, , x \in \mathbb{R}^d \tag{8}$$

is (E, H)-operator scaling with stationary increments as soon as $H \in (0, \min_{1 \leq j \leq d} \lambda_j)$. Its semi-variogram is therefore given by

$$\forall x \in \mathbb{R}^d, \; v_{_{X_\psi}}(x) = \frac{1}{2} \int_{\mathbb{R}^d} \left| e^{i\langle x, \xi \rangle} - 1 \right|^2 \psi(\xi)^{-2H-q} d\xi.$$

A moving average representation is also obtained, choosing M a real Gaussian random measure with Lebesgue control measure and $\varphi : \mathbb{R}^d \to [0, \infty)$ a continuous, E-homogeneous function such that $\varphi(x) \neq 0$ for $x \neq 0$, under an additional assumption of (β, E)-admissibility (see Definition 2.7

of [10]), by considering

$$X_\varphi(x) = \int_{\mathbb{R}^d} \left(\varphi(x-y)^{H-q/\alpha} - \varphi(-y)^{H-q/2}\right) M(dy)\ , x \in \mathbb{R}^d, \tag{9}$$

for $H \in (0, \beta)$. In this case, its semi-variogram is given by

$$\forall x \in \mathbb{R}^d,\ \ v_{X_\varphi}(x) = \frac{1}{2}\int_{\mathbb{R}^d} \left|\varphi(x-y)^{H-q/\alpha} - \varphi(-y)^{H-q/2}\right|^2 dy.$$

Several examples for ψ or φ are given. In particular, when E is a diagonalizable matrix with positive eigenvalues $\lambda_1, \ldots, \lambda_d$, one can choose $\theta_1, \ldots, \theta_d$ the eigenvectors for E^t such that $E^t\theta_i = \lambda_i\theta_i$ for $i = 1, \ldots, d$ that form a basis of $\mathbb{R}^d$. Let us introduce $a_i = 1/\lambda_i$, $1 \le i \le 1$, then the function

$$\tau_E(x) = \left(\sum_{i=1}^d |\langle x, \theta_i\rangle|^{2a_i}\right)^{1/2},\ x \in \mathbb{R}^d, \tag{10}$$

is a continuous E-homogeneous and β-admissible for convenient β (see Corollary 2.12 of [10] fore more details and generalizations).

Let us remark that the set

$$S_E := \{x \in \mathbb{R}^d; \tau_E(x) = 1\}$$

is bounded (it follows for instance from Corollary 3.4 of [9]). Thus, using also continuity of τ_E, we obtain that S_E is a compact set of $\mathbb{R}^d$. Hence, defining for $x \neq 0$, the direction $\ell_E(x) = \tau_E(x)^{-E}x \in S_E$ we obtain the unique "E-radial" decomposition of x as

$$x = \tau_E(x)^E \ell_E(x),$$

with $(\tau_E(x), \ell_E(x)) \in (0, +\infty) \times S_E$. Let us mention that (τ_E, ℓ_E) corresponds to the polar coordinates introduced in Lemma 6.1.5 of [28]: here the difference is that explicit expressions of S_E and τ_E are known, whereas Lemma 6.1.5 ibid establishes their existence. Then the operator scaling property implies that

$$v_{X_\psi}(x) = \tau_E(x)^{2H} v_{X_\psi}(\ell_E(x)) \ \text{ as well as } \ v_{X_\varphi}(x) = \tau_E(x)^{2H} v_{X_\varphi}(\ell_E(x)),$$

for all $x \in \mathbb{R}^d$ (since $X_\psi(0) = X_\varphi(0) = 0$ a.s.). However the explicit computation of v_{X_ψ} or v_{X_φ} are not known in general (see also Remark 4.3 of [10]). Our main result in this section gives assumption in order to use τ_E^{2H} as a semi-variogram function.

Theorem 1. *Let E be a real $d \times d$ diagonalizable matrix with eigenvalues $a_1^{-1}, \ldots, a_d^{-1} \in [1, +\infty)$ and eigenvectors $\theta_1, \ldots, \theta_d$ such that $E^t\theta_i = a_i^{-1}\theta_i$, for every $1 \le i \le d$. For $H \in (0, 1]$, define the function $v_{E,H} : \mathbb{R}^d \to \mathbb{R}_+$ by*

$$\forall x \in \mathbb{R}^d,\ v_{E,H}(x) = \tau_E(x)^{2H} \tag{11}$$

with τ_E defined by (10).

1. *Then there exists a real-valued centered Gaussian random field $X_{E,H} = \{X_{E,H}(x); x \in \mathbb{R}^d\}$ with stationary increments such that*

$$\forall x, y \in \mathbb{R}^d,\ \frac{1}{2}\mathbb{E}\Big[\big(X_{E,H}(x) - X_{E,H}(y)\big)^2\Big] = v_{E,H}(x-y).$$

   In other words, $v_{E,H}$ is the semi-variogram function of the random field $X_{E,H}$.
2. *Moreover, the random field $X_{E,H}$ is also (E, H)-operator scaling.*

Proof. Let us consider d independent fractional Brownian motions $\left\{B_{a_i}^{(i)}(t); t \in \mathbb{R}\right\}$ with respective Hurst index a_i for $1 \le i \le d$ and semi-variogram given by (5) that is by

$$\forall t, s \in \mathbb{R},\ v_{B_{a_i}^{(i)}}(t) = \frac{1}{2}\mathbb{E}\left(\left(B_{a_i}^{(i)}(t+s) - B_{a_i}^{(i)}(s)\right)^2\right) = |t|^{2a_i}.$$

Note that when $a_i = 1$, the fractional Brownian motion B_{a_i} with Hurst index a_i may be defined as $B^{(i)}_{a_i}(t) = tZ_i$ for $Z_i \sim \mathcal{N}(0,2)$. Let us now consider the random field Y defined by

$$\forall x \in \mathbb{R}^d,\ Y(x) = \sum_{i=1}^{d} B^{(i)}_{a_i}(\langle x, \theta_i\rangle).$$

Then Y has stationary increments and its semi-variogram is given by

$$\gamma(x) = \frac{1}{2}\mathbb{E}\Big[(Y(x+h) - Y(h))^2\Big] = \sum_{i=1}^{d} |\langle x, \theta_i\rangle|^{2a_i} = \tau_{_E}(x)^2$$

for any $x, h \in \mathbb{R}^d$. As a semi-variogram, γ is then a function of negative type, i.e. for all integer $n \in \mathbb{N}\backslash\{0\}$, for all $x^{(1)}, \ldots, x^{(n)} \in \mathbb{R}^d$ and for all $\lambda_1, \ldots, \lambda_n \in \mathbb{R}$ such that $\sum_{i=1}^n \lambda_i = 0$, we have:

$$\sum_{i=1}^{n}\sum_{j=1}^{n} \lambda_i\lambda_j\gamma\Big(x^{(i)} - x^{(j)}\Big) \leq 0.$$

By Lemma 2.1 of [22] using Schoenberg Theorem, since $H \in (0,1]$, $v_{_{E,H}} = \gamma^H$ is also a function of negative type and thus it is the semi-variogram of a real-valued centered random field $X_{_{E,H}}$ with stationary increments. The second assertion of the theorem simply follows from the fact that $\tau_{_E}$ is an E-homogeneous function. □

Remark 1. *Note that, for all $C_1, \ldots, C_d$ non-negative constants, we can prove similarly that the function $x \mapsto \left(\sum_{i=1}^d C_i|\langle x, \theta_i\rangle|^{2a_i}\right)^{1/2}$ is a semi-variogram.*

In the case where the eigenvalues of E are all equals, we can write for $x = (x_1, \ldots, x_d) \in \mathbb{R}^d$,

$$v_{_{E,H}}(x) = c_\alpha(x)^{\alpha H}, \tag{12}$$

where $c_\alpha(x) = \left(\sum_{i=1}^d |x_i|^\alpha\right)^{1/\alpha}$ corresponds to the α-(quasi)-norm for some $\alpha \in (0,2]$. It follows that $E = \frac{2}{\alpha} I_d$ and the Gaussian random field $X_{_{E,H}}$ is $\frac{\alpha}{2}H$-self-similar. Moreover, $X_{_{E,H}}$ is anisotropic for $\alpha \neq 2$. This provides new examples of topothesy functions (see Figures 3 and 4) as considered in [17], that also could be useful for spatial modelling, see for instance [2].

Let us conclude this section with some sample path properties of the operator scaling random field with semi-variogram $v_{_{E,H}}$ (see [9]) implying their fractal properties.

Proposition 1. *Let $K = [0,1]^d$ and let $X_{_{E,H}}$ be a centered Gaussian random field with stationary increments and semi-variogram $v_{_{E,H}}$ defined by* (11)*. Then there exists a modification $X^*_{_{E,H}}$ of $X_{_{E,H}}$ on K satisfying the two following assertions.*

(1) *For any $\varepsilon > 0$*

$$\lim_{\delta\downarrow 0} \sup_{\substack{x,y\in K\\ 0<\|x-y\|\leq\delta}} \frac{\Big|X^*_{_{E,H}}(x) - X^*_{_{E,H}}(y)\Big|}{\tau_{_E}(x-y)|\log \tau_{_E}(x-y)|^{1/2+\varepsilon}} = 0 \text{ almost surely}$$

where $\tau_{_E}$ is given by (10)*.*

(2) *For all $i = 1, \ldots, d$, for any $\varepsilon > 0$*

$$\lim_{\delta\downarrow 0} \sup_{\substack{x+t\tilde{\theta}_i, x+s\tilde{\theta}_i\in K\\ 0<|t-s|\leq\delta}} \frac{\Big|X^*_{_{E,H}}(x+t\tilde{\theta}_i) - X^*_{_{E,H}}(x+s\tilde{\theta}_i)\Big|}{|t-s|^{H_i}|\log|t-s|^{H_i}|^{1/2+\varepsilon}} = 0 \text{ almost surely,}$$

where $\tilde{\theta}_1, \ldots, \tilde{\theta}_d$ are the unit eigenvectors of E such that $E\tilde{\theta}_i = a_i^{-1}\tilde{\theta}_i$ and $H_i = Ha_i$ for $1 \leq i \leq d$.

Let us quote that exact moduli of continuity for harmonizable operator-scaling Gaussian random fields have been established in Theorem 4.2 of [25]. The proof of this result highly relies on the existence of a spectral density from which strong local nondeterminism properties are deduced. Let us quote that $X_{E,H}$ may not admit an harmonizable representation as X_ψ. Actually, it is not difficult to see that for $H = 1$, the spectral measure $X_{E,H}$ is not absolutely continuous with respect to Lebesgue measure. We refer to [4] for the interested reader.

In particular $X_{E,H}$ gives an interesting example of Gaussian random field with stationary increments that may admit particular directions in which its regularity is greater. This could be of importance for some applications in medical imaging. For instance, such a behavior is observed on trabecular bone radiographs, for which fractal analysis allows to improve osteoporosis diagnosis (see [5, 7] for example).

Let us also quote that when $X_{E,H}$ is (E,H)-operator scaling, for any invertible matrix $P \in GL(\mathbb{R}^d)$ the random field $X_{E,H}(P\,\cdot)$ is $(P^{-1}EP, H)$-operator scaling. Hence, in the sequel we restrict our simulation study to the case where E is diagonal.

3. Fast and exact Method of Simulation

3.1. **Method of the circulant embedding matrix.** Let us briefly describe the circulant embedding matrix method for simulations of stationary Gaussian processes and fields.

Case of stationary processes $d = 1$.
We consider $(Y(t))_{t\in\mathbb{R}}$ a centered stationary Gaussian process with covariance function given by

$$\forall t, s \in \mathbb{R},\ r(t) = \mathbb{E}(Y(t+s)Y(s)).$$

In order to simulate the centered Gaussian vector

$$y = (Y(t_0), Y(t_1), \dots, Y(t_N)),$$

where $\mathcal{G} := \{t_0, \dots, t_N\} \subset \mathbb{R}^{N+1}$ is an ordered subspace of points in $\mathbb{R}$ with constant mesh $t_{i+1} - t_i$, one has to consider the covariance matrix of y (identified with the column vector) given by

$$R := (r(|t_j - t_i|))_{0\le i,j\le N}.$$

Using Choleski decomposition, one can find a lower triangular matrix A such that $R = AA^t$ and $y \overset{d}{=} A\epsilon$ for $\epsilon \sim \mathcal{N}(0, I_{N+1})$. The cost to find A of the order $\mathcal{O}(N^3)$ may be quickly prohibitive. However, due to stationarity and equispaced grid, the matrix R is a Toeplitz matrix meaning that $R_{i,j}$ only depends on $i - j$. In this case the embedding circulant method consists in embedding R in a circulant matrix that is diagonalized by the Discrete Fourier Transform matrix. More precisely, due to Toeplitz structure, R is entirely characterized by its first column

$$r = (r_0, r_1, \dots, r_N),\ \text{with } r_k = r(|x_k - x_0|) \text{ for } k = 0 \dots N,$$

Let us consider an integer $M \ge N$. One can construct a symmetric circulant matrix $S \in \mathcal{M}_{2M}(\mathbb{R})$ by defining its first column $s \in \mathbb{R}^{2M}$ such that

$$\begin{cases} s_0 = r_0 \\ s_k = s_{2M-k} = r_k,\ 1 \le k \le N-1. \end{cases}$$

In addition, if $M > N$, $s_{N+1}, \dots, s_{2M-N}$ are arbitrarily (or artfully) chosen such that $s_j = s_{2M-j}$ for $j = 1 \dots 2M-1$. Then

$$S = \sum_{k=0}^{2M-1} s_k T_{2M}^k = \sum_{k=0}^{N} r_k T_{2M}^k + \sum_{k=N+1}^{2M-N} s_k T_{2M}^k + \sum_{k=1}^{N-1} r_k T_{2M}^{2M-k},$$

with T_{2M} the circulant $2M \times 2M$ matrix defined by

$$\begin{cases} T_{2M} f_j = f_{j+1},\ 1 \le j \le 2M-1 \\ T_{2M} f_{2M} = f_1, \end{cases}$$

where $(f_1, \dots, f_{2M})$ is the canonical basis of $\mathbb{R}^{2M}$. Recall that

$$T_{2M}^t = T_{2M}^{2M-1},\ T_{2M}^{2M} = I_{2M}$$

and that the powers of T_{2M} generate the set of $2M \times 2M$ circulant matrices. Note that R is embedded in S since $(S_{i,j})_{0 \le i,j \le N} = R$.
Now, let us recall that a circulant matrix is diagonalized by the matrix of discrete Fourier transform in such a way that its eigenvalues are also given by the discrete Fourier transform of its first row. More precisely, let us denote by F_{2M} the discrete Fourier matrix defined by

$$F_{2M} = \frac{1}{\sqrt{2M}} \left(\omega_{2M}^{(k-1)(l-1)}\right)_{0 \le k,l \le 2M}$$

with $\omega_{2M} = e^{-i\pi/M} \in \mathbb{C}$ and recall that $F_{2M}\overline{F_{2M}^t} = I_{2M}$. Since S is circulant one has

$$S = \overline{F_{2M}^t}\mathrm{diag}(F_{2M}s)F_{2M}.$$

Writing $\tilde{s} = F_{2M}s$, the matrix S is a covariance matrix if and only if its eigenvalues are non negative meaning that $\tilde{s} \ge 0$ in the sense that $\tilde{s}_j \ge 0$ for all $j = 1, \dots, 2M$.

In such a case, one may obtain two independent copies of y by considering

$$\tilde{y}^{(1)} = \Re(A_{2M}(\epsilon_1 + i\epsilon_2)) \text{ and } \tilde{y}^{(2)} = \Im(A_{2M}(\epsilon_1 + i\epsilon_2)),$$

with ϵ_1 and ϵ_2 two independent Gaussian vectors with common distribution $\mathcal{N}(0, I_{2M})$ and

$$A_{2M} = \overline{F_{2M}^t}(\mathrm{diag}(\tilde{s}))^{1/2} = F_{2M}^{-1}(\mathrm{diag}(\tilde{s}))^{1/2}$$

such that $S = A_{2M}\overline{A_{2M}}^t$ and $\tilde{y}^{(1)}$ and $\tilde{y}^{(2)}$ are independent vectors of distribution $\mathcal{N}(0, S)$. Hence restricting to the $N+1$ first entries we get two independent copies of y.

The minimal embedding method consists in choosing $M = N$ and

$$s = (r_0, r_1, \dots, r_N, r_{N-1}, \dots, r_1).$$

In this case, it follows that for $l \in \{1, \dots, 2N\}$,

$$\widetilde{s_l} = \frac{1}{\sqrt{2N}} \left(r_0 + (-1)^l r_N + 2\sum_{k=1}^{N-1} r_k \cos\left(2\pi \frac{kl}{2N}\right)\right). \tag{13}$$

Hence, as soon as $\widetilde{s_l} \ge 0$ for all $l \in \{1, \dots, 2N\}$, using N as a power of two, the Fast Fourier transform allows to reduce the cost of simulation to $\mathcal{O}(N \log(N))$. In [19], several assumptions on r are given to provide this non-negativeness assumption. One can also include a test of non-negativeness in the algorithm to ensure that S is a covariance matrix. Note that it implies also that R should be a covariance matrix. A well adapted situation is when Y is also periodic. Actually, if Y is periodic of period $T > 0$, its covariance function also satisfies $r(t + T) = r(t)$, for $t \in \mathbb{R}$. Hence considering, $t_k = \frac{kT}{2N}$ for $k = 0, \dots, 2N-1$, the minimal circulant embedding matrix S of R is exactly the covariance matrix of the Gaussian vector $(Y(t_0), Y(t_1), \dots, Y(t_N), \dots, Y(t_{2N-1}))$.

Case of stationary fields $d = 2$.
Let us consider now a stationary centered Gaussian random field in dimension $d = 2$ given by $Y = \{Y(x,y); (x,y) \in \mathbb{R}^2\}$, with covariance function

$$\forall (x,y), (x',y') \in \mathbb{R}^2,\ r(x,y) = \mathbb{E}(Y(x+x', y+y')Y(x',y')),$$

satisfying the additional assumption that $r(x,y) = r(|x|,|y|)$. To simulate the Gaussian vector

$$\{Y(x_p, y_q); 0 \le p, q \le N\}$$

of size $(N+1)^2$ corresponding to the values of Y on a rectangular grid $\mathcal{G} = \{(x_p, y_q); 0 \le p, q \le N\}$ with constant mesh, one can order this vector using lexicographical order. Then its covariance matrix R is block Toeplitz with each block being also Toeplitz. The matrix R is characterized by its first column constituted by blocks

$$(R_0, R_1, \dots, R_N),$$

where

$$R_k = (\mathbb{E}(Y(x_i, y_k)Y(x_j, y_0)))_{0\leq i,j\leq N} = (r(x_i - x_j, y_k - y_0))_{0\leq i,j\leq N}$$

is symmetric due to the additional assumption on r. Each block R_k may be embedded in a minimal symmetric circulant matrix $S_k \in \mathcal{M}_{2N}(\mathbb{R})$. Hence the minimal symmetric circulant embedding matrix of R, denoted by S, is defined by its first block column given by

$$(S_0, S_1, \ldots, S_N, S_{N-1}, \ldots, S_1)\,.$$

Now, eigenvectors of S are given by the 2-dimensional discrete Fourier matrix and its eigenvalues are computed by the 2-dimensional discrete Fourier transform of the periodized matrix

$$K_{per} = \begin{pmatrix} K & K_1 \\ K_2 & K_3 \end{pmatrix}, \tag{14}$$

where

$$\begin{cases} K = (r(x_i - x_0, y_j - y_0))_{0\leq i,j\leq N}\,, \\ K_1 = (r(x_i - x_0, y_{N-j} - y_0))_{0\leq i\leq N, 1\leq j\leq N-1}\,, \\ K_2 = (r(x_{N-i} - x_0, y_j - y_0))_{1\leq i\leq N-1, 0\leq j\leq N} \\ K_3 = (r(x_{N-i} - x_0, y_{N-j} - y_0))_{1\leq i,j\leq N-1} \end{cases}$$

Hence, when the 2-dimensional discrete Fourier transform of K_{per} is non-negative, one can simply used the spectral decomposition of S in order to simulate Y. Note that when Y is periodic of period $T > 0$ in each coordinate, its covariance function also satisfies $r(x+T, y+T) = r(x, y)$, for $(x, y) \in \mathbb{R}^2$. Hence considering, $x_k = y_k = \frac{kT}{2N}$ for $k = 0, \ldots, 2N-1$, the minimal circulant embedding matrix S of R is exactly the covariance matrix of the Gaussian vector $(Y(t_0), Y(t_1), \ldots, Y(t_N), \ldots, Y(t_{2N-1}))$ such that the 2-dimensional discrete Fourier transform of the periodized matrix K_{per} is non-negative.

3.2. **Simulation of OSGRF for $H = 1$.** Let us recall that we can restrict our study to the case of a diagonal matrix E.

Let $E = \mathrm{diag}(1/a_1, \ldots, 1/a_d)$ with $a_1, \ldots, a_d \in (0, 1]$ and $X_{E,1}$ be an operator scaling centered Gaussian random field with semi-variogram $v_{E,1} = \tau_E{}^2$ for τ_E defined by (10). It follows that

$$\{X_{E,1}(x); x \in \mathbb{R}^d\} \overset{(fdd)}{=} \left\{ \sum_{i=1}^{d} B^{(i)}_{a_i}(\langle x, e_i\rangle); x \in \mathbb{R}^d \right\},$$

with $B^{(1)}_{a_1}, \ldots, B^{(d)}_{a_d}$ independent fractional Brownian motions with respective Hurst indices $a_1, \ldots, a_d$ and $(e_1, \ldots, e_d)$ the canonical basis of $\mathbb{R}^d$. Here the semi-variogram of the fractional Brownian motion B_a with Hurst index a is given by (5) for $H = a$. We recall that for $a = 1$ and $Z \sim \mathcal{N}(0, 2)$, we simply have $\{B_a(t); t \in \mathbb{R}\} \overset{(fdd)}{=} \{tZ; t \in \mathbb{R}\}$. Now, for $a \in (0, 1)$, the fractional Brownian motion B_a is not a stationary process but we may consider the associated fractional Gaussian noise

$$Y_a = \{B_a(t + 1) - B_a(t); t \in \mathbb{R}\},$$

which is a stationary process with covariance function given by

$$\mathrm{Cov}(Y_a(t), Y_a(s)) = r_a(|t - s|) \text{ with } r_a(t) = |t + 1|^{2a} - 2|t|^{2a} + |t - 1|^{2a}.$$

Hence, we may consider the method of the circulant embedding matrix described in Section 3.1 to simulate the centered Gaussian vector $(Y_a(0), \ldots, Y_a(N))$, with covariance matrix

$$R_a = (r_a(|j - i|))_{0\leq i,j\leq N}\,, \tag{15}$$

using $t_j = j$ for $0 \leq j \leq N$, as done in [15]. Let us recall the main result of [30], also stated in [16]: for all $a \in (0, 1)$, $N \geq 1$ and $l \in \{1, \ldots, 2N\}$,

$$\frac{1}{\sqrt{2N}} \left(r_a(0) + (-1)^l r_a(N) + 2 \sum_{k=1}^{N-1} r_a(k) \cos\left(2\pi \frac{kl}{2N}\right) \right) \geq 0.$$

In other words, since the eigenvalues of the minimal circulant embedding matrix S_a of R_a are given by (13), the symmetric circulant matrix S_a is the covariance matrix of a centered Gaussian random vector $\widetilde{Y_a} = \left(\widetilde{Y_a}(0,\dots,\widetilde{Y_a}(2N-1)\right)$ and there is no need to check numerically the non-negativity of its eigenvalues.

It follows that the method of the circulant embedding matrix can always be used for the synthesis of a fBm on an equispaced interval (see Algorithm 1 in appendix). Actually using stationarity of the increments and self-similarity of B_a and the fact that $B_a(0) = 0$ a.s., one has for any step $\delta > 0$

$$\{B_a(\delta k); 0 \le k \le N\} \stackrel{d}{=} \delta^a \left\{ \sum_{j<k} Y_a(j); 0 \le k \le N \right\} \stackrel{d}{=} \delta^a \left\{ \sum_{j<k} \widetilde{Y}_a(j); 0 \le k \le N \right\},$$

with the convention that $\sum_{j<0} = 0$. Hence, in dimension $d = 2$ for instance, one has simply exact simulation of the $(E,1)$-operator scaling random field $X_{_{E,1}}$ on the grid $\mathcal{G} = \{(\delta i, \delta j); 0 \le i,j \le N\}$ with a cost $O(N\log(N))$ using

$$\left\{X_{_{E,1}}(\delta i, \delta j); 0 \le i,j \le N\right\} \stackrel{d}{=} \left\{B^{(1)}_{a_1}(\delta i) + B^{(2)}_{a_2}(\delta j); 0 \le i,j \le N\right\}.$$

In the sequel we investigate the case where $H \in (0,1)$.

3.3. **Simulation of OSGRF for $H \in (0,1)$ and $E = I_d$: Stein Method for fBf.** When $E = I_d$ and $H \in (0,1)$, the operator scaling centered Gaussian random field $X_{_{E,H}}$ with semi-variogram $v_{_{E,H}} = {\tau_{_E}}^2$ for τ_E defined by (10) is simply a fractional Brownian field, which is an isotropic field. To simulate it, [34] proposes to contruct it owing a stationary isotropic Gaussian random field Y whose semi-variogram is closed enough to the fBf one. More precisely, for $H \in (0,1)$, [34] introduces the compactly supported continuous function

$$k_H(r) = \begin{cases} c_H - r^{2H} + (1-c_H)r^2 & \text{if } r \le 1 \\ 0 & \text{else} \end{cases}$$

where $c_H \in (0,1)$. The main idea is then to choose the constant c_H such that $K_H(x) := k_H(\|x\|)$, $x \in \mathbb{R}^d$, is a radial continuous isotropic covariance, which means that

$$(x,y) \mapsto k_H(\|x-y\|)$$

is a covariance function on $\mathbb{R}^d \times \mathbb{R}^d$. Then this function is mapped to a function $\overline{K}_H$ defined on $\mathbb{R}^d$, which has periodicity 2 in each coordinate, satisfying

$$\forall x \in [-1,1]^d,\ \overline{K}_H(x) = K_H(x). \tag{16}$$

Theorem 2 in [34] asserts that for $c_H = 1-H$, K_H is a covariance function on $\mathbb{R}^d$ for $d \le 3$, as soon as $H \in (0,1/2]$. Theorem 3 ibid. states that when $d \le 2$, this remains valid for $H \in (1/2, 3/4]$. Let us quote a mistake in the proof of Theorem 2 in [34]: in equation (A.1), a term in cosinus is missing and we were not able to correct this proof taking into account this term. However, we give here an alternative proof.

Theorem 2. *Let $H \in (0,1/2]$ and $c_H = 1-H$. Then, for $d \le 3$, the isotropic function $K_H(x) := k_H(\|x\|)$, $x \in \mathbb{R}^d$, is a covariance function.*

Proof. Our proof uses a d-dimensional isotropic extension of Polya's 1949 result about positive definiteness of even function, convex on $[0,+\infty)$ and vanishing at infinity, due to [3]. Note that Schoenberg [32] gives a complete characterization of the class of functions that are radial and positive definite on $\mathbb{R}^d$ for all $d \in \mathbb{N}$. In particular, such functions are linked to completely monotone functions according to Hausdorff-Bernstein-Widder theorem and can not be compactly supported. A weaker notion of complete monotony, called multiply monotony has been introduced: a function $\varphi : (0,+\infty) \to \mathbb{R}^d$ is l-multiply monotone, with $l \ge 2$, if it is $\mathcal{C}^{l-2}$ and $(-1)^j\varphi^{(j)}$ is non-negative, non-increasing and convex for all $j = 0,\dots,k-2$. Due to Askey [3], it follows that such a function may define a radial positive function on $\mathbb{R}^d$, for all $[d/2] \le l-2$ (see also [20]). Hence, the theorem will follow from the 3-multiply monotony of the function k_H, which means that $k_H \in \mathcal{C}^1(0,+\infty)$ with k_H and $-k'_H$

non-negative, non-decreasing and convex on $(0,+\infty)$. First let us remark that k_H is continuous on $(0,+\infty)$ and is differentiable on $(0,1)\cup(1,+\infty)$, with, for all $r\in(0,1)$

$$k'_H(r) = -2Hr^{2H-1} + 2(1-c_H)r.$$

Since $1-c_H = H$, we get that k_H is also differentiable at point $r=1$ with $k'_H(1)=0$, ensuring that k'_H is continuous on $(0,+\infty)$ and therefore $k_H\in\mathcal{C}^1((0,+\infty))$.
When $H=1/2$, we clearly get that $-k'_H(r) = 2H(1-r)_+$ is non-negative, non-increasing and convex so that k_H is also convex and non-increasing. Since k_H is a non-increasing function with compact support, it is also non-negative.
Moreover, for $H\in(0,1/2)$, $k_H\in\mathcal{C}^3((0,1)\cup(1,+\infty))$, with for $r\in(0,1)$,

$$k_H^{(2)}(r) = -2H(2H-1)r^{2H-2} + 2(1-c_H) \text{ and } k_H^{(3)}(r) = -4H(2H-1)(H-1)r^{2H-3}.$$

It follows that, $k_H^{(3)}(r)\le 0$ for all $r\in(0,1)\cup(1,+\infty)$ and $k_H^{(2)}$ is non-increasing on $(0,1)\cup(1,+\infty)$. Hence $k_H^{(2)}(r)\ge k_H^{(2)}(1) = 4H(1-H)\ge 0$ for $r\in(0,1)$ and $k_H^{'}$ is non-decreasing and concave on $(0,+\infty)$. Finally, since $k'_H(r)\le k'_H(1)=0$, we also get that k_H is non-increasing and convex on $[0,+\infty)$. This proves that k_H is 3-times monotone and concludes the proof. □

Following the one dimensional case stated in Corollary p.631 of [21], using Poisson formula, the periodic function $\overline{K}_H$, given by (16), is a continuous covariance, as soon as K_H is a continuous covariance. Moreover, since it is periodic, the method of the circulant embedding matrix described in Section 3.1 in dimension $d=2$, allows to simulate exactly, on an equispaced square grid of $[0,2]^2$, the stationary Gaussian centered random field Y_H with covariance $\overline{K}_H$, i.e. such that

$$\forall x,y\in\mathbb{R}^d,\ \mathbb{E}(Y_H(x)Y_H(y)) = \overline{K}_H(x-y).$$

To simulate B_H the fBf of order H, whose semi-variogram is given by (5), [34] then remarks that

$$\left\{B_H(x)\,;\ x\in[0,\frac{1}{\sqrt{2}}]^2\right\} \overset{(fdd)}{=} \left\{Y_H(x)-Y_H(0)+\sqrt{1-c_H}(x_1G_1+x_2G_2);\ x=(x_1,x_2)\in[0,\frac{1}{\sqrt{2}}]^2\right\}$$

where G_1,G_2 are two independent Gaussian random variables with common law $\mathcal{N}(0,2)$ and are independent of Y_H. Algorithm 2 (see the appendix), applied with $a_1=a_2=1$, leads to the simulation of B_H on the grid $\mathcal{G}=\{(\delta i,\delta j);0\le i,j\le N\}$ with a cost $O\big(N^2\log(N)\big)$.

3.4. **Simulation of OSGRF for $H\in(0,1)$ and E diagonal.** In the general case where

$$E = \mathrm{diag}(a_1^{-1},a_2^{-1},\dots,a_d^{-1})$$

for $a_i\in(0,1]$ for all i, we consider anisotropic generalization of previous results by substituting the Euclidean norm $\|\cdot\|$ with $\tau_{_E}$ defined by (10), that is we define $K_{_{E,H}}(x) := k_H(\tau_{_E}(x))$ by

$$K_{_{E,H}}(x) = \begin{cases} c_H - \tau_{_E}(x)^{2H} + (1-c_H)\tau_{_E}(x)^2 & \text{if } \tau_{_E}(x) := \left(\sum_{i=1}^d |x_i|^{2a_i}\right)^{1/2}\le 1 \\ 0 & \text{else.}\end{cases}$$

Let us quote that $\{x\in\mathbb{R}^d;\tau_{_E}(x)\le 1\}\subset[-1,1]^d$ so that $K_{_{E,H}}$ has compact support included in $[-1,1]^d$. Then we may define the function $\overline{K}_{_{E,H}}$ on $\mathbb{R}^d$, which has periodicity 2 in each coordinate, satisfying

$$\forall x\in[-1,1]^d,\ \overline{K}_{_{E,H}}(x) = K_{_{E,H}}(x).$$

Theorem 3. *Assume that $K_{_{E,H}}$ is the covariance function of a stationary centered Gaussian random field. Then, there exists a periodic stationary centered Gaussian random field $Y_{_{E,H}}$ such that*

$$\forall x,y\in\mathbb{R}^d,\ \mathbb{E}\big(Y_{_{E,H}}(x)Y_{_{E,H}}(y)\big) = \overline{K}_{_{E,H}}(x-y).$$

Let $B_{a_i}^{(i)}$, $1\le i\le d$, be d independent fractional Brownian motions, with respective index a_i, that is with respective semi-variograms defined by (5). Assume that this family $\left\{B_{a_i}^{(i)}\,;\,1\le i\le d\right\}$ and $Y_{E,H}$

are independent. Then define the random field Z by

$$\forall x=(x_1,\dots,x_d)\in\mathbb{R}^d,\ Z_{E,H}(x)=Y_{E,H}(x)-Y_{E,H}(0)+\sqrt{1-c_H}\sum_{i=1}^{d}B_{a_i}^{(i)}(x_i).$$

Let $M\in[0,1]$ be defined by

$$M=\min\left\{0\le r\le 1\,;\,\sum_{i=1}^{d}|r|^{2a_i}\le 1\right\}.$$

Then $\left\{Z_{E,H}(x);x\in[0,M]^d\right\}\overset{(fdd)}{=}\left\{X_{E,H}(x);x\in[0,M]^d\right\}$, where we recall that $X_{E,H}$ is defined in Theorem 1.

Proof. If $K_{E,H}$ is a covariance function, since it has compact support, as already remarked in the previous section, using Poisson formula and Bochner Theorem (see chapter XIX [21] for instance), this implies that $\overline{K}_{E,H}$ is also a covariance function. Hence one may define $Y_{E,H}$ as a periodic stationary centered Gaussian random field with covariance function given by $\overline{K}_{E,H}$. Since $B_{a_i}^{(i)}$, $1\le i\le d$ and $Y_{E,H}$, are independent centered Gaussian random field with stationary increments, $Z_{E,H}$ is also a centered Gaussian random field with stationary increments. Let us compute its semi-variogram, which is defined on $\mathbb{R}^d$. Let $x=(x_1,\dots,x_d)\in\mathbb{R}^d$ and first note that $Z_{E,H}(0)=0=X_{E,H}(0)$ almost surely. By independence of the random fields $B_{a_i}^{(i)}$, $1\le i\le d$ and $Y_{E,H}$

$$\begin{aligned}\tfrac{1}{2}\mathbb{E}\Big(\big(Z_{E,H}(x)-Z_{E,H}(0)\big)^2\Big) &= \frac{1}{2}\mathbb{E}\left(\left(Y_{E,H}(x)-Y_{E,H}(0)+\sqrt{1-c_H}\sum_{i=1}^{d}B_{a_i}^{(i)}(x_i)\right)^2\right)\\ &= \frac{1}{2}\mathbb{E}\Big(\big(Y_{E,H}(x)-Y_{E,H}(0)\big)^2\Big)+\frac{1-c_H}{2}\sum_{i=1}^{d}\mathbb{E}\left(\left(B_{a_i}^{(i)}(x_i)\right)^2\right)\\ &= \overline{K}_{E,H}(0)-\overline{K}_{E,H}(x)+(1-c_H)\sum_{i=1}^{d}|x_i|^{2a_i}\end{aligned}$$

Therefore,

$$\frac{1}{2}\mathbb{E}\Big(\big(Z_{E,H}(x)-Z_{E,H}(0)\big)^2\Big)=c_H-\overline{K}_{E,H}(x)+(1-c_H)\tau_E(x)^2.$$

As soon as $x\in[-M,M]^d$, $\tau_E(x)\le 1$, and then by definition of $\overline{K}_{E,H}$ and $K_{E,H}$,

$$\frac{1}{2}\mathbb{E}\Big(\big(Z_{E,H}(x)-Z_{E,H}(0)\big)^2\Big)=\tau_E(x)^{2H}=v_{E,H}(x).$$

This implies that, for $z,y\in[0,M]^d$,

$$\mathrm{Cov}(Z_{E,H}(z),Z_{E,H}(y))=v_{E,H}(z)+v_{E,H}(y)-v_{E,H}(z-y)=\mathrm{Cov}(X_{E,H}(z),X_{E,H}(y)),$$

which concludes the proof. □

As in the case of fBf (which corresponds to $E=I_d$), the method of the circulant embedding matrix described in Section 3.1 in dimension $d=2$, allows to simulate exactly, on an equispaced square grid of $[0,2]^2$, the stationary Gaussian centered random field $Y_{E,H}$ with covariance $\overline{K}_{E,H}$, and then to simulate the operator scaling Gaussian random field $X_{E,H}$ (using Theorem 3) with a cost $O\big(N^2\log(N)\big)$ (see Algorithm 2 in the appendix).

4. Numerical study

4.1. **Procedure and comments.** In our numerical study, we focus on operator scaling random fields $X_{E,H}$ in dimension $d = 2$ and with $H \neq 1$. The first part of our numerical study focus on the range of valid parameters. Let us note that the random field $X_{E,H}$ can be parametrized either by (a_1, a_2, H) or by (H_1, H_2, H) where $H_1 = a_1 H$ and $H_2 = a_2 H$ prescribe the sample path smoothness (see Proposition 1). The parametrization (a_1, a_2, H) allows to fix the anisotropic quasi-norm τ_E, choosing a_1 and a_2: the directional Hölder regularity will then depend on H.

In lots of practical applications, especially in medical imaging, self-similarity or Hölder regularity exponents are used as indicators (see [26] for instance). Hence, the parametrization (H_1, H_2, H) may be more relevant: it allows to fix the Hölder regularity properties and to study the anisotropy by letting the parameter H varies. The assumptions $a_1 \in (0,1)$, $a_2 \in (0,1)$ and $H \in (0,1)$ rewrite as $H_1 \in (0,1)$, $H_2 \in (0,1)$ and $H \geq \max(H_1, H_2)$. In the self-similar case, where $a_1 = a_2 = \alpha/2 \in (0,1]$ or equivalently $H_1 = H_2$, the semi-variogram is given by a power of the α-(quasi)-norm (see (12)). Self-similarity is given by $\frac{\alpha}{2}H$ for $H \in (0,1)$ while anisotropy is controlled by $\alpha \in (0,2)$, the case where $\alpha = 2$ corresponding to isotropic fractional Brownian fields. A specific attention is given to this case in Section 4.2.2.

The first numerical results concern the range of parameters (H_1, H_2, H) (or (α, H) for self-similar fields) for which the circulant embedding method is valid on a specific grid of points in order to simulate $X_{E,H}$ (see Section 4.1.1). Then, for the numerical evaluation of our proposed algorithm, we compare the empirical semi-variogram obtained by a Monte-Carlo estimation with the theoretical one (see Section 4.1.2) and perform estimation of the Hölder exponents $H_1 = a_1 H$ and $H_2 = a_2 H$ (see Section 4.1.3). Numerical results are presented in Section 4.2.

4.1.1. *Range of valid parameters.* Let us first quote that, for simulation purpose, Theorem 3 may be weaken in a discrete setting. Actually, if $N \geq 1$ and $d = 2$, we have for $a_1, a_2, H \in (0,1)$ and $E = \mathrm{diag}(a_1^{-1}, a_2^{-1})$,

$$\Big\{X_{E,H}(x); x \in \big([0,M] \cap N^{-1}\mathbb{Z}\big)^2\Big\} \overset{(fdd)}{=} \Big\{Z_{E,H}(x); x \in \big([0,M] \cap N^{-1}\mathbb{Z}\big)^2\Big\},$$

where for all $x = (x_1, x_2) \in ([0,1] \cap N^{-1}\mathbb{Z})^2$,

$$Z_{E,H}(x) = Y_{E,H}(x) - Y_{E,H}(0) + \sqrt{1 - c_H} B^{(1)}_{a_1}(x_1) + \sqrt{1 - c_H} B^{(2)}_{a_2}(x_2).$$

and

$$M = \inf\Big\{r \in (0,1] \,/\, r^{2H_1/H} + r^{2H_2/H} \leq 1\Big\}.$$

The Gaussian random vector

$$\Big\{Y_{E,H}\Big(\frac{k}{N}, \frac{l}{N}\Big); \quad 0 \leq k, l \leq 2N-1\Big\}$$

is well-defined as soon as the circulant matrix of size $2N \times 2N$ defined by its first column constituted by blocks $(S_0, S_1, \ldots, S_{2N-1})$, where

$$S_k = \left(\overline{K}_{E,H}\left(\frac{i-j}{N}, \frac{k}{N}\right)\right)_{0 \leq i,j \leq 2N-1},$$

is positive definite. Since eigenvalues of this matrix are given by the 2-dimensional Fourier transform of size $2N \times 2N$, we check numerically non-negativeness of these eigenvalues, which is enough to simulate the realization of the vector

$$\Big\{X_{E,H}\Big(\frac{k}{N}, \frac{l}{N}\Big); \quad 0 \leq k, l \leq [NM]\Big\}$$

where $[y]$ denotes the integer part of y. We have computed the minimum of these eigenvalues in function of the parameters $(H_1, H_2, H) \in (0,1)^3$ discretizing the interval $(0,1)$ on a regular grid with mesh $\Delta = 0.01$. Let us also emphasize that an other important issue is the size $([NM]+1)^2$ of the discretized generated image: since the anisotropic quasi-norm τ_E varies with the parameters (H_1, H_2, H), this size also varies and then we also compute it with respect to the parameters.

Choosing $N = 2^{10}$, Figure 1 presents the range of the parameters (H_1, H_2, H), for which our algorithm works and the size of the obtained images. More precisely, Figure 1 (a) associates to each valid parameter (H_1, H_2, H) the size $[MN]$ and Figures 1 (b)–(e) correspond to cross-sections for special values of H; the last figure presents the largest image that one can generate for prescribed smoothness properties, i.e. if the only parameters of interest are (H_1, H_2). When H increases, the range of admissible parameters (H_1, H_2) also increases: in other words, once (H_1, H_2) is chosen, it seems that there exists a critical value H_c such that for any $H > H_c$ the algorithm works. In addition, once (H_1, H_2) is chosen, the greater H is, the smaller the generated image is. And according to Figure 1 (f), when the sample directional regularities are prescribed, one can generate an important image, up to choose well H.

Figure 2 illustrates the specific case of self-similar random fields ($H_1 = H_2 = \alpha H/2$), giving the size of the generated image in term of valid parameters (α, H). When the Euclidean norm ($\alpha = 2$) is replaced by an anisotropic α-(quasi)-norm ($\alpha \in (0, 2)$), the range of valid H seems to increase whereas the image size is lower. As already mentionned, α-(quasi)-norms provide new examples of topothesy functions as considered in [17] and Figures 3 and 4 illustrate their behavior.

4.1.2. *Comparison of empirical and theoretical semi-variograms.* The empirical semi-variogram $v_{E,H}^{emp}$ is computed using $n = 5000$ realizations of the operator scaling random field $X_{E,H}$ on an equispaced grid with mesh $N = 2^{10}$. Hence the empirical semi-variogram $v_{E,H}^{emp}$ is also evaluated on this equispaced grid, that is at $([NM])^2$ points and we compare it with the theoretical semi-variogram $v_{E,H}^{emp}$ computing the mean relative error

$$MRE = \frac{1}{([NM])^2} \sum_{i=1}^{[NM]} \sum_{j=1}^{[NM]} \frac{\left| v_{E,H}^{emp}\left(\frac{i}{N}, \frac{j}{N}\right) - v_{E,H}\left(\frac{i}{N}, \frac{j}{N}\right) \right|}{v_{E,H}\left(\frac{i}{N}, \frac{j}{N}\right)}$$

on the grid.

We first illustrate the case $H_1 = H_2 = \frac{\alpha}{2} H$ (see Figures 5–7), which corresponds to self-similar random fields $X_{E,H}$ with Hurst index H_1. As expected, since the simulation algorithm is exact in principle, the error MRE is reasonable, meaning that the empirical semi-variogram fits well the theoretical one. In this framework, the Hölder regularity does not vary with the direction: the pointwise Hölder exponent in direction θ is always H_1. In particular, when $\alpha = 2$, $H = H_1 = H_2$, τ_E is the Euclidean norm and the simulated random field $X_{E,H}$ is the isotropic fractional Brownian field with Hurst index H_1. These figures allow to illustrate the anisotropic structure when the isotropic Euclidean norm $\|\cdot\|$ is replaced by an anisotropic α-quasi-norm for $\alpha = 2H_1/H$. Note that even for H closed to H_1, the anisotropic structure appears on the realization. Moreover, when $H \to 1_-$, the structure looks like a sheet, this follows from the fact that the limit field $X_{E,1}$ is given

$$X_{E,1}(x_1, x_2) = B_{H_1}^{(1)}(x_1) + B_{H_2}^{(2)}(x_2) \tag{17}$$

with $B_{H_1}^{(1)}$ and $B_{H_2}^{(2)}$ two independent fractional Brownian motions.

Then Figures 8–10 are devoted to examples of operator scaling random fields $X_{E,H}$ with different directional regularity (that is $H_1 \neq H_2$). The mean relative error MRE is still reasonable. Note that in this case, all the simulated fields are anisotropic and the direction in which the field is greater (the vertical one choosing $H_2 \geq H_1$) is always perceptible on the realizations. Moreover, as in the self-similar framework, when $H \to 1_-$, we recover the sheet structure of $X_{E,1}$, corresponding to the sum of two independent fractional Brownian motions (17).

4.1.3. *Parameter estimation using quadratic variations.* Let us now briefly introduce estimators we used for the parameters H_1 and H_2. Considering a realization of

$$\left\{ X_{E,H}\left(\frac{k}{N}, \frac{l}{N}\right); \quad 0 \leq k, l \leq [NM] \right\}$$

by our method of simulation, we can compute for $u \in \mathbb{N}\backslash\{0\}$

$$V^{(1)}_{N,u}(k) = \frac{1}{[NM]-2u+1} \sum_{l=0}^{[NM]-2u} \left(X_{E,H}\left(\frac{l+2u}{N}, \frac{k}{N}\right) - 2X_{E,H}\left(\frac{l+u}{N}, \frac{k}{N}\right) + X_{E,H}\left(\frac{k}{N}, \frac{l}{N}\right)\right)^2,$$

that corresponds to the quadratic variations of second order of the horizontal line process

$$L^{(1)}_k := \left\{ X_{E,H}\left(t, \frac{k}{N}\right); t \in \mathbb{R} \right\}.$$

Note that $L^{(1)}_k - L^{(1)}_k(0)$ is simply a fractional Brownian motion on $\mathbb{R}$ with Hurst index given by $H_1 = a_1 H$. Since this is true for all $k \leq [NM]$, we consider the mean of this quadratic variations given by

$$V^{(1)}_{N,u} = \frac{1}{[NM]+1} \sum_{k=0}^{[NM]} V^{(1)}_{N,u}(k).$$

Our estimator of H_1 is then defined by

$$\widehat{H_{1,N}} = \frac{1}{2\log\left(\frac{u}{v}\right)} \log\left(\frac{V^{(1)}_{N,u}}{V^{(1)}_{N,v}}\right),$$

where we set $u = 2$ and $v = 1$ in experiments. Let us quote that since the order of variations is $K = 2 > H + d/4$ in dimension $d = 2$ for any $H \in (0,1)$, adaptation of the proof of Theorem 4.1 of [8], stated in terms of spectral density, should allow to prove asymptotic normality of this estimator, but this is not the purpose of the present paper. Similarly we consider

$$\widehat{H_{2,N}} = \frac{1}{2\log\left(\frac{u}{v}\right)} \log\left(\frac{V^{(2)}_{N,u}}{V^{(2)}_{N,v}}\right),$$

with $([NM]+1)([NM]-2u+1)V^{(2)}_{N,u}$ given by

$$\sum_{l=0}^{[NM]-2u} \left(X_{E,H}\left(\frac{k}{N}, \frac{l+2u}{N}\right) - 2X_{E,H}\left(\frac{l+u}{N}, \frac{k}{N}\right) + X_{E,H}\left(\frac{k}{N}, \frac{l}{N}\right)\right)^2.$$

Note that the vertical line processes $L^{(2)}_k := \left\{X_{E,H}(k/N, t); t \in \mathbb{R}\right\}$ are such that $L^{(2)}_k - L^{(2)}_k(0)$ is a fractional Brownian motion on $\mathbb{R}$ with Hurst index given by $H_2 = a_2 H$, for any $k \in \mathbb{N}$. The results of estimation are presented for $N = 2^{10}$ on 100 realizations in Tables 1–6. The estimators perform very well, which suggests that the discretized simulation allows to recover the sample path regularity properties. Note the standard deviation increases with H: this should be due to the image size which is lower when H increases.

4.2. **Numerical results.**

4.2.1. *Range of valid parameters and topothesy.*

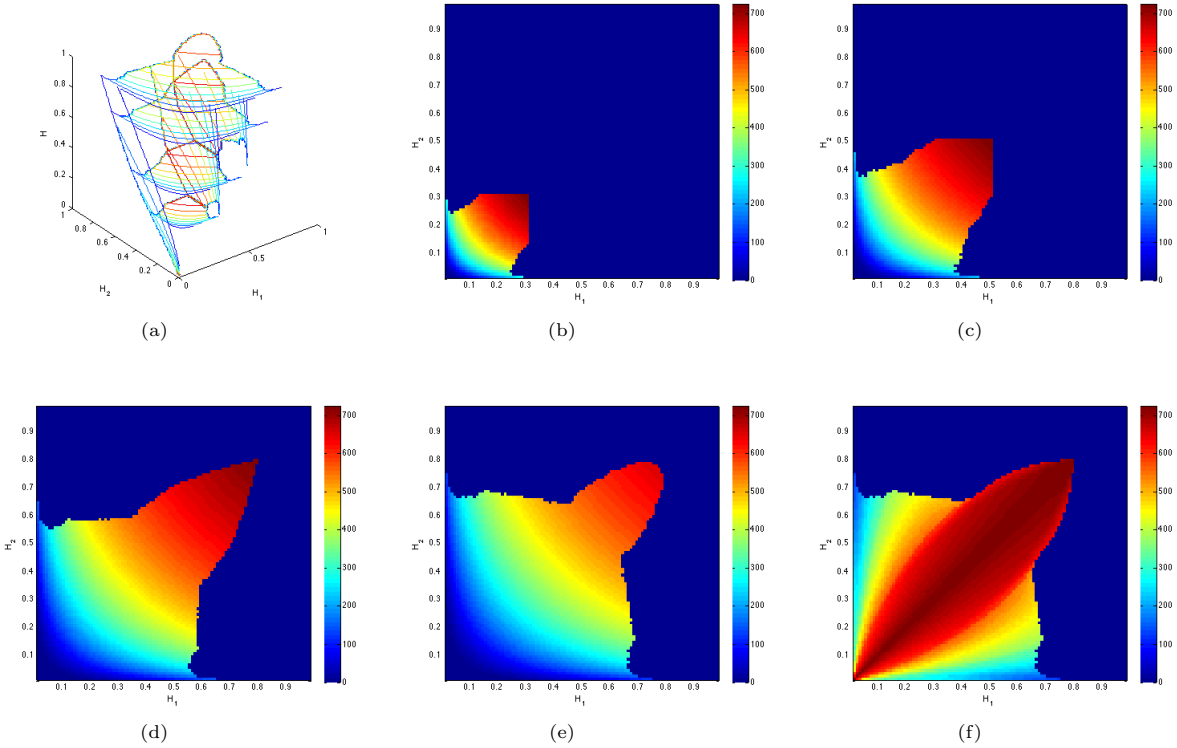

FIGURE 1. Contour plots of the size $[MN]$ of the generated image. From top to the bottom: (a) in function of (H_1, H_2, H); (b) in plane $H = 0.3$; (c) in plane $H = 0.5$; (d) in plane $H = 0.8$; (e) in plane $H = 0.99$; (f) Maximum size in function of (H_1, H_2).

4.2.2. *Self-similar framework ($H_1 = H_2$).*

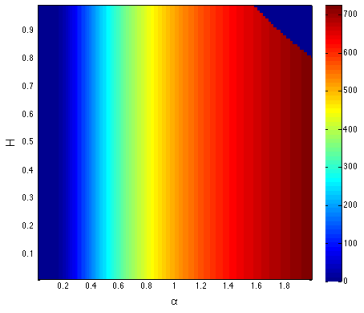

FIGURE 2. Image size $[MN]$ of the generated image in function of (α, H) with $\alpha = 2a_1$, $H_1 = H_2 = \alpha H/2$

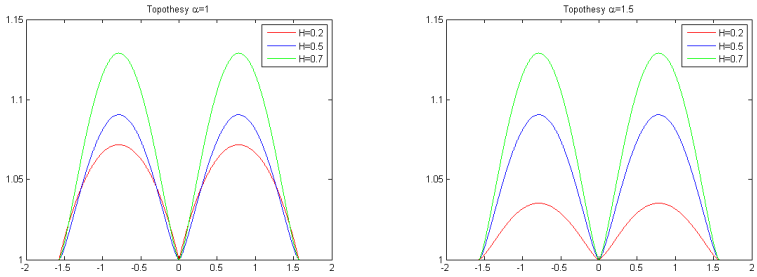

FIGURE 3. Topothesy function $\theta \mapsto (|\cos(\theta)|^\alpha + |\sin(\theta)|^\alpha)^H$ for $\theta \in [-\pi/2, \pi/2]$ corresponding to $\theta \mapsto c_\alpha \left((\cos(\theta), \sin(\theta))\right)^{\alpha H}$ for semi-variogram of $\alpha H/2$ self-similar random fields given by (12)

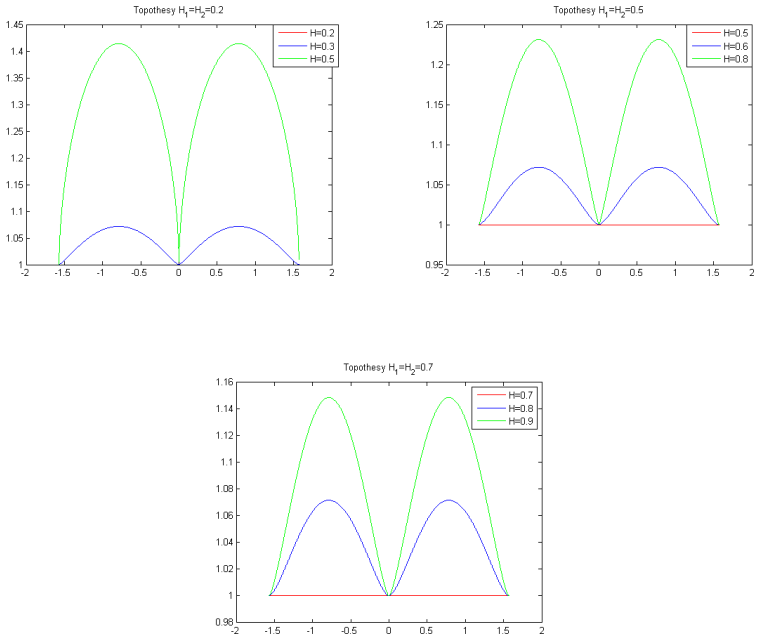

FIGURE 4. Topothesy function $\theta \mapsto (|\cos(\theta)|^\alpha + |\sin(\theta)|^\alpha)^H$ for $\theta \in [-\pi/2, \pi/2]$ corresponding to $\theta \mapsto c_\alpha \left((\cos(\theta), \sin(\theta))\right)^{\alpha H}$ for semi-variogram of $H_1 = H_2$ self-similar random fields given by (12) with $\alpha = 2H_1/H$

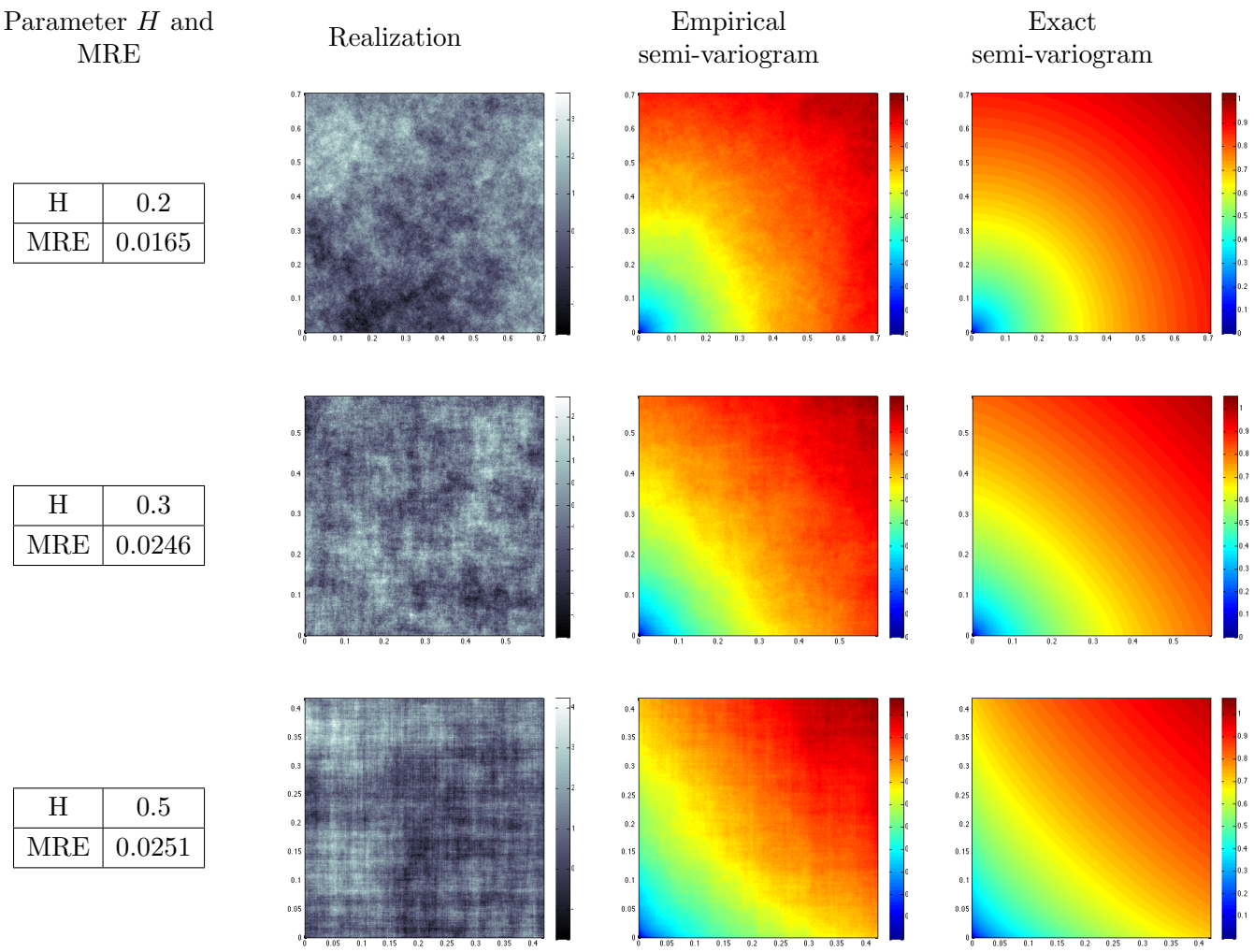

FIGURE 5. OSGRF with $H_1 = H_2 = 0.2$

	$H = 0.2$	$H = 0.3$	$H = 0.5$	$H = 0.7$	$H = 0.9$
$\widehat{H_1}$	0.2001 ± 0.0019	0.1998 ± 0.0027	0.1987 ± 0.0071	0.1997 ± 0.0278	0.1997 ± 0.0688
$\widehat{H_2}$	0.1999 ± 0.0022	0.1994 ± 0.0026	0.1987 ± 0.0058	0.2003 ± 0.0271	0.2037 ± 0.0661
$[MN]$	724	608	430	304	215

TABLE 1. Estimation of H_1 and H_2 using quadratic variations on 100 realizations with a mesh size $N = 2^{10}$; Exact values of the parameters $H_1 = H_2 = 0.2$

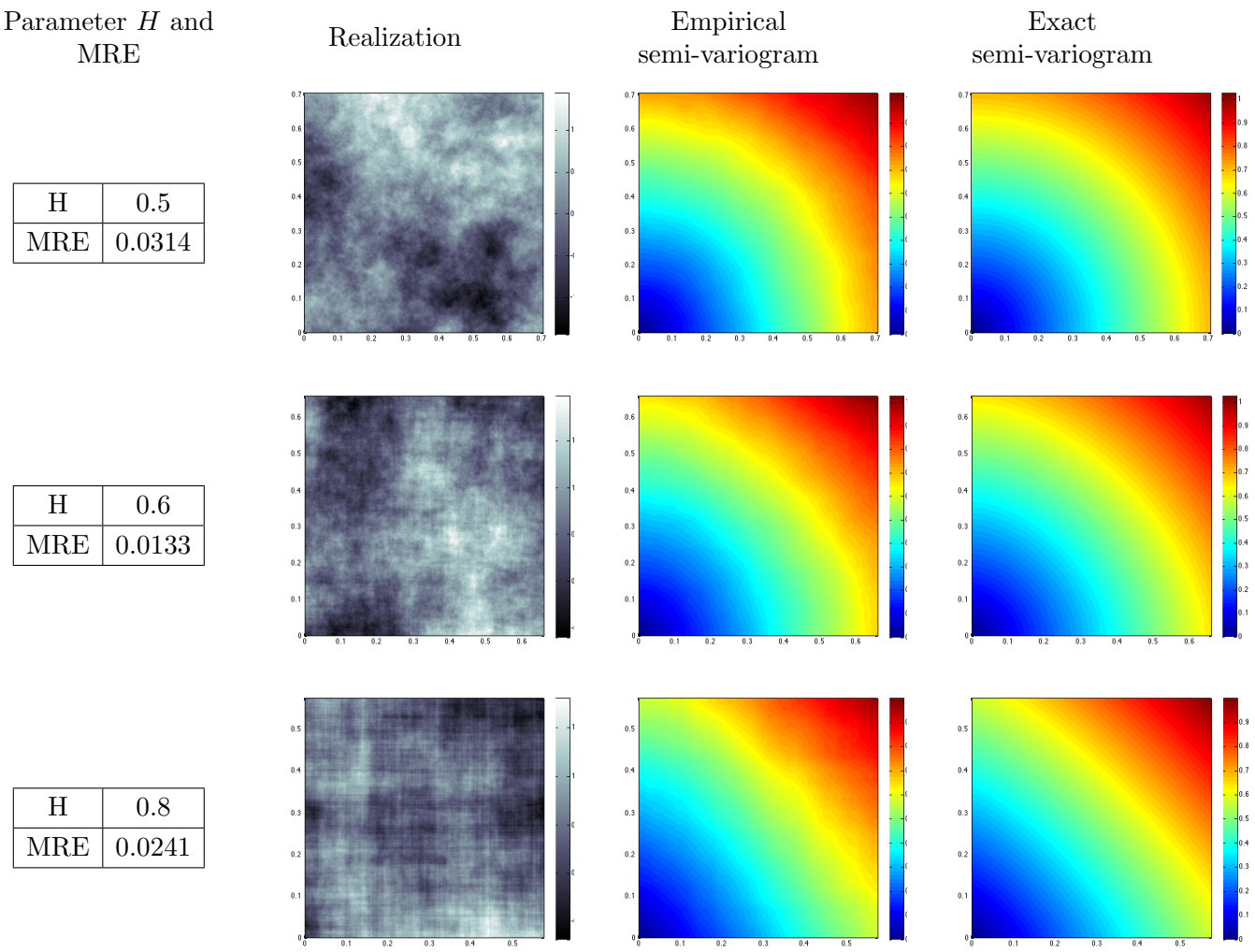

FIGURE 6. OSGRF with $H_1 = H_2 = 0.5$

	$H = 0.5$	$H = 0.6$	$H = 0.7$	$H = 0.8$	$H = 0.9$
$\widehat{H_1}$	0.4998 ± 0.0021	0.5000 ± 0.0030	0.4996 ± 0.0050	0.4996 ± 0.0119	0.5046 ± 0.0301
$\widehat{H_2}$	0.5000 ± 0.0020	0.5003 ± 0.0027	0.5000 ± 0.0055	0.5002 ± 0.0118	0.4986 ± 0.0362
$[MN]$	724	675	630	588	548

TABLE 2. Estimation of H_1 and H_2 using quadratic variations on 100 realizations with a mesh size $N = 2^{10}$; Exact values of the parameters $H_1 = H_2 = 0.5$

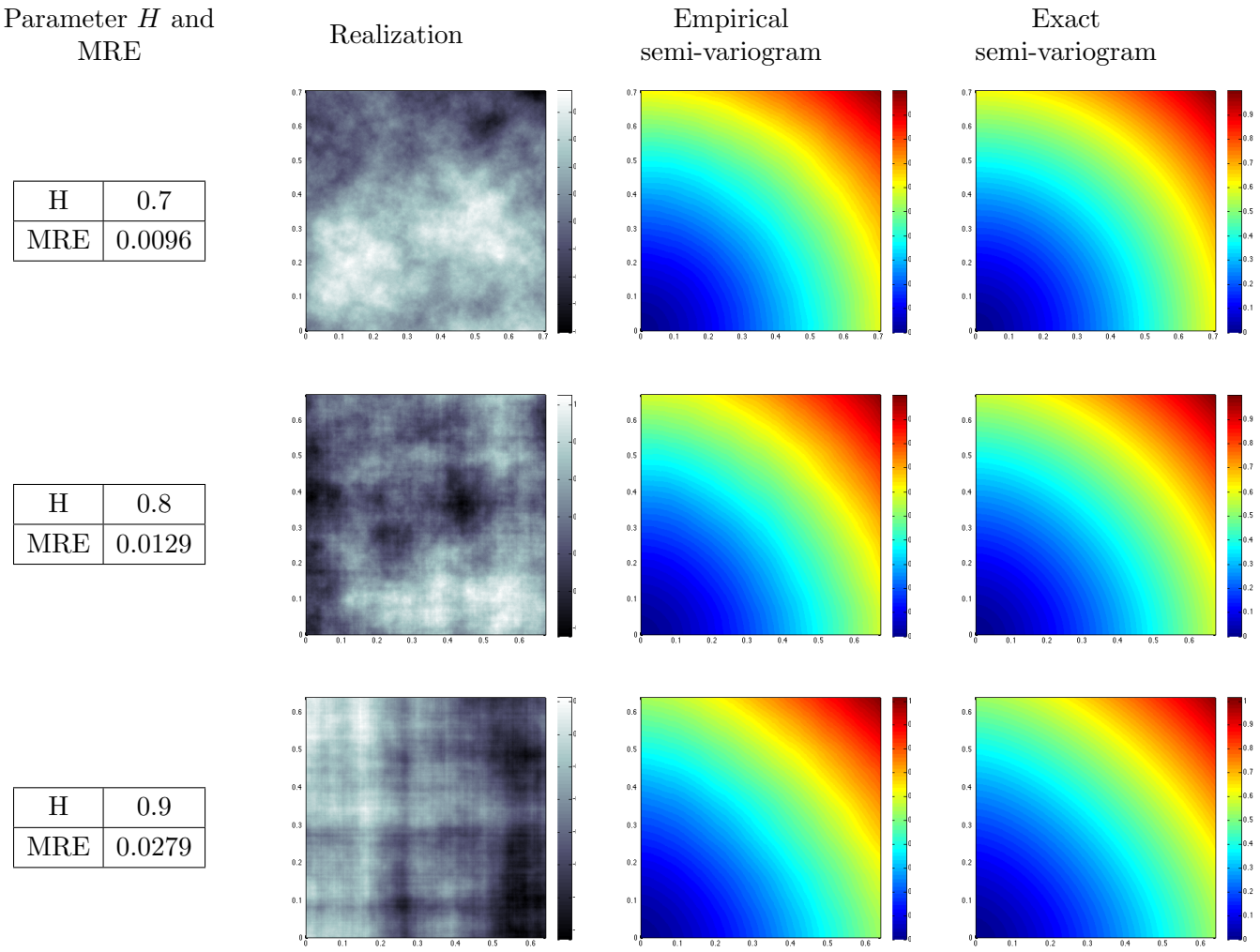

FIGURE 7. OSGRF with $H_1 = H_2 = 0.7$

	$H = 0.7$	$H = 0.8$	$H = 0.9$
$\widehat{H_1}$	0.6997 ± 0.0022	0.6990 ± 0.0047	0.7014 ± 0.0167
$\widehat{H_2}$	0.7001 ± 0.0021	0.7002 ± 0.0048	0.6991 ± 0.0194
$[MN]$	724	689	655

TABLE 3. Estimation of H_1 and H_2 using quadratic variations on 100 realizations with a mesh size $N = 2^{10}$; Exact values of the parameters $H_1 = H_2 = 0.7$

4.2.3. *Operator scaling fields with $H_1 \neq H_2$.*

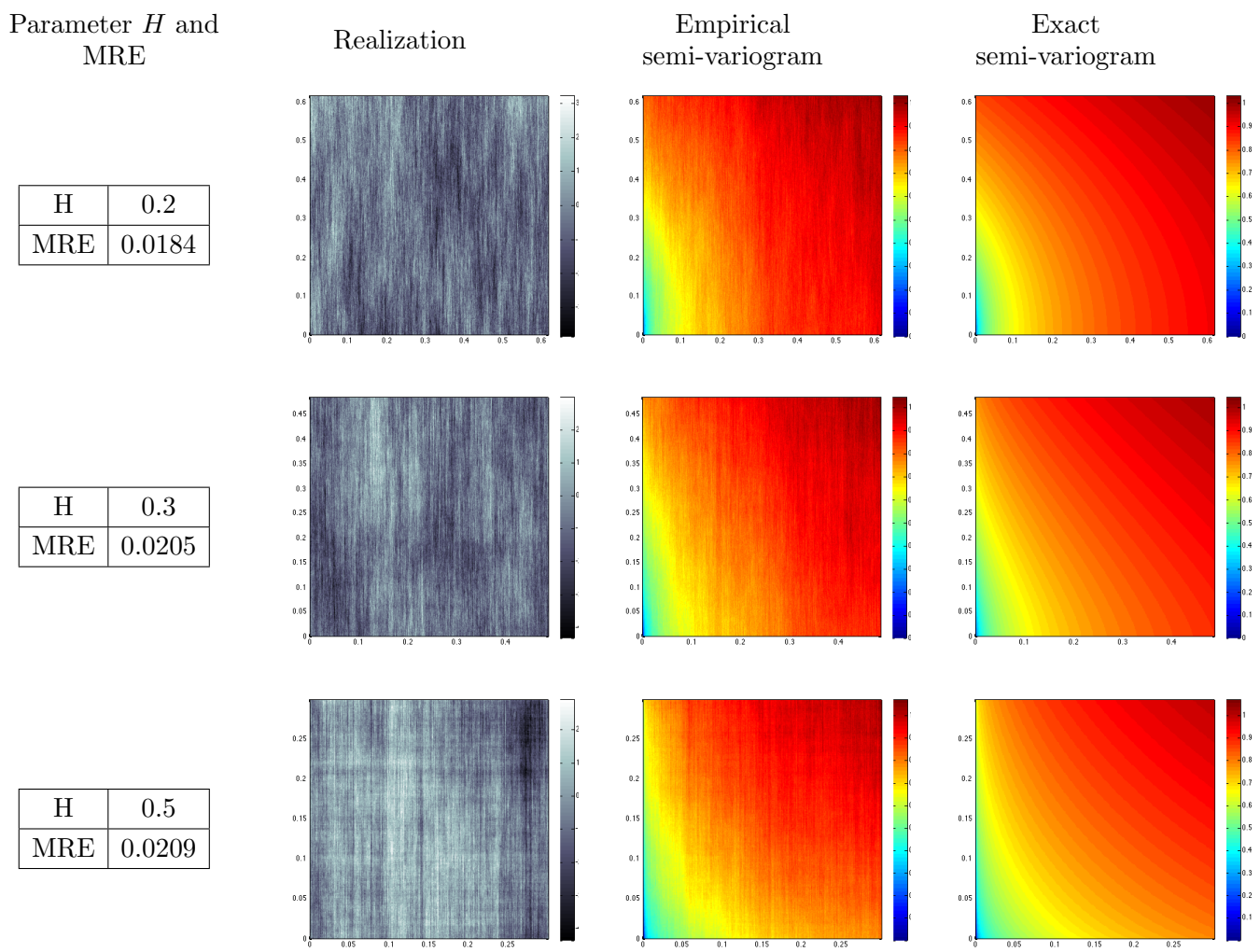

FIGURE 8. OSGRF with $H_1 = 0.1$, $H_2 = 0.2$

	$H = 0.2$	$H = 0.3$	$H = 0.5$	$H = 0.7$	$H = 0.9$
$\widehat{H_1}$	0.1022 ± 0.0078	0.1032 ± 0.0109	0.0981 ± 0.0302	0.0995 ± 0.0717	0.1076 ± 0.1089
$\widehat{H_2}$	0.1997 ± 0.0022	0.2004 ± 0.0032	0.2005 ± 0.0061	0.2016 ± 0.0319	0.2041 ± 0.1098
$[MN]$	632	497	307	190	117

TABLE 4. Estimation of H_1 and H_2 using quadratic variations on 100 realizations with a mesh size $N = 2^{10}$; Exact values of the parameters $H_1 = 0.1$ and $H_2 = 0.2$

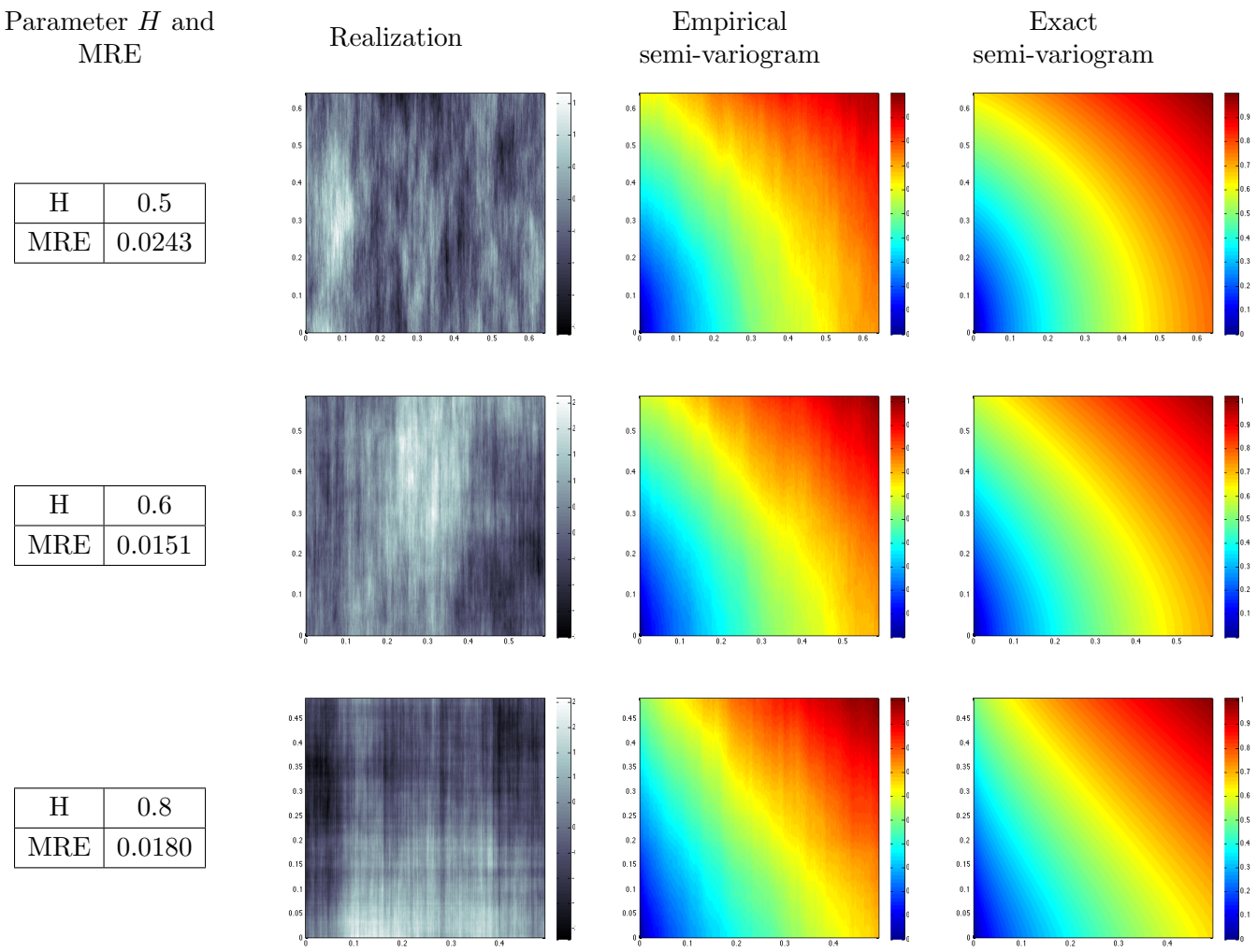

FIGURE 9. OSGRF with $H_1 = 0.3$, $H_2 = 0.5$

	$H = 0.5$	$H = 0.6$	$H = 0.7$	$H = 0.8$	$H = 0.9$
$\widehat{H_1}$	0.3003 ± 0.0099	0.2990 ± 0.0143	0.3046 ± 0.0207	0.3018 ± 0.0316	0.2990 ± 0.0520
$\widehat{H_2}$	0.5000 ± 0.0022	0.4999 ± 0.0024	0.4998 ± 0.0044	0.5004 ± 0.0115	0.5045 ± 0.0299
$[MN]$	657	601	550	504	461

TABLE 5. Estimation of H_1 and H_2 using quadratic variations on 100 realizations with a mesh size $N = 2^{10}$; Exact values of the parameters $H_1 = 0.3$ and $H_2 = 0.5$

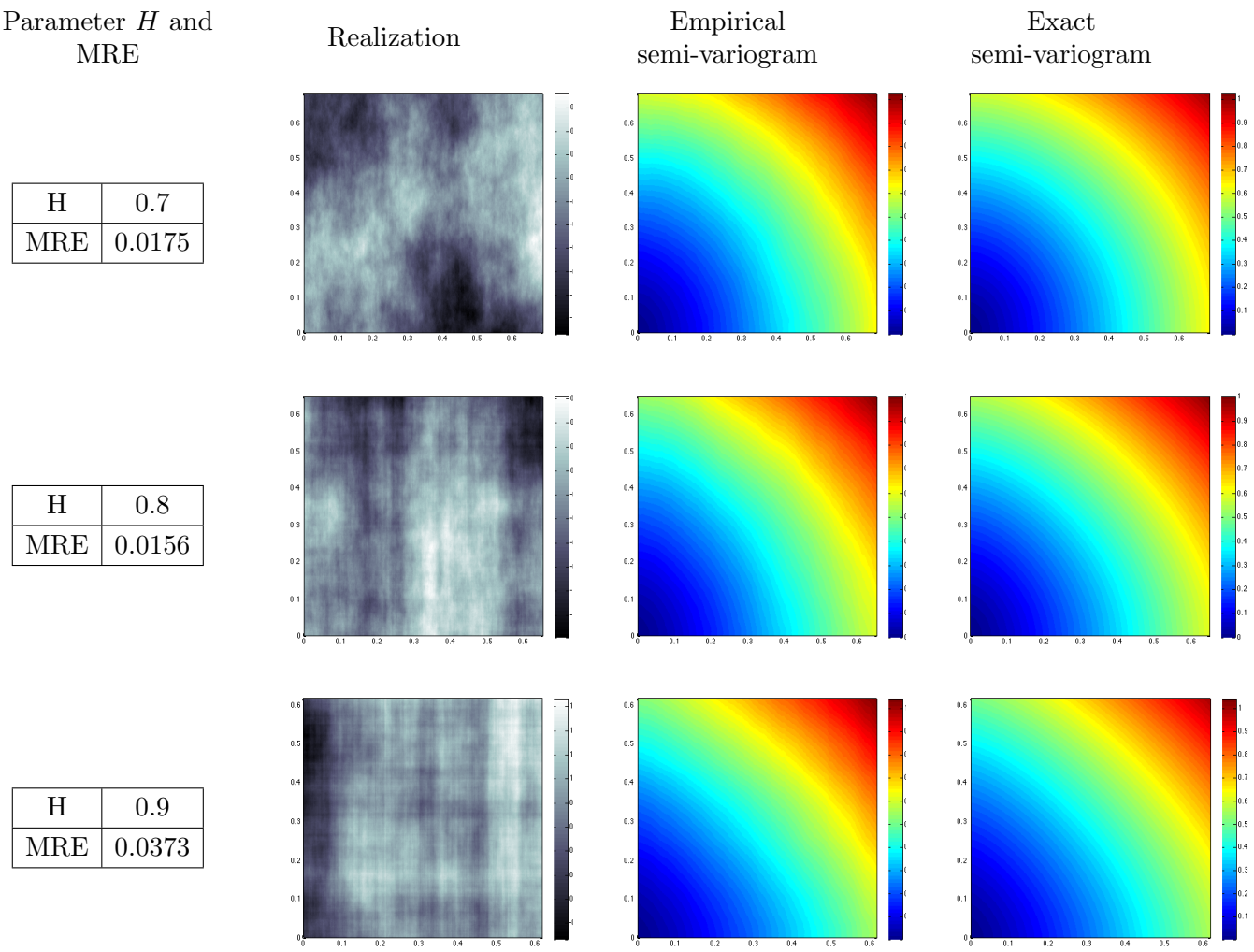

FIGURE 10. OSGRF with $H_1 = 0.6$, $H_2 = 0.7$

	$H = 0.7$	$H = 0.8$	$H = 0.9$
$\widehat{H_1}$	0.6002 ± 0.0046	0.5992 ± 0.0103	0.6014 ± 0.0231
$\widehat{H_2}$	0.7002 ± 0.0019	0.6995 ± 0.0048	0.7000 ± 0.0157
$[MN]$	704	667	633

TABLE 6. Estimation of H_1 and H_2 using quadratic variations on 100 realizations with a mesh size $N = 2^{10}$; Exact values of the parameters $H_1 = 0.6$ and $H_2 = 0.7$

Appendix A. Algorithms

Algorithm 1 Simulation of fractional Brownian motion with Hurst parameter a on $[0,1]$.

Inputs:
$N \leftarrow$ mesh size parameter (e.g. $N = 2^9$) .
$a \leftarrow$ Hurst parameter

Step 1. Compute the first line of the covariance matrix $\boldsymbol{R_a}$ defined by (15)
for $k = 0$ to N **do**
  $r(k) \leftarrow N^{-2a}\Big((k+1)^{2a} - 2k^{2a} + |k-1|^{2a}\Big)$
end for

Step 2. Compute the first line of the minimal embedding covariance matrix $\boldsymbol{S_a}$
for $k = 0$ to N **do**
  $s(k) \leftarrow r(k)$
  $s(N+1+k) \leftarrow r(N-1-k)$
end for

Step 3. Compute the eigenvalues $\boldsymbol{\tilde{s}_1, \ldots, \tilde{s}_{2N}}$ of $\boldsymbol{S_a}$
$\tilde{s} \leftarrow \mathrm{FFT}(s)$ ▷ we use the normalization associated with FFT command of Matlab

Step 4. Simulation of the periodic random field $\boldsymbol{\widetilde{Y}_a}$
$\varepsilon_1 \leftarrow$ Generate a vector with law $\mathcal{N}(0, I_{2N})$
$\varepsilon_2 \leftarrow$ Generate a vector with law $\mathcal{N}(0, I_{2N})$
$\widetilde{Y}_a \leftarrow \Re\Big(\sqrt{2N}\,\mathrm{IFFT}((\varepsilon_1 + i\varepsilon_2).*\sqrt{\tilde{s}}\Big)$
▷ we use the normalization associated with inverse FFT command of Matlab

Step 5. Compute the FBM $\boldsymbol{B_a}$
Initialize : $B_a(0) \leftarrow 0$
for $k = 1$ to N **do**
  $B_a(k) \leftarrow \widetilde{Y}_a(0) + \ldots + \widetilde{Y}_a(k-1)$
end for

Output: B_a discretized FBM with Hurst index a

Algorithm 2 Simulation of OSGRF $X_{E,H}$.

Inputs:
$N \leftarrow$ mesh size parameter (e.g. $N = 2^9$) .
$H, a_1, a_2 \leftarrow$ parameters of the covariance functions of $X_{E,H}$

Step 1. Compute the periodized matrix $\boldsymbol{K_{per}}$ defined by (14)
for $i = 0$ to N **do**
  for $j = 0$ to N **do**
    $K_{per}(i,j) \leftarrow c_H - \tau_E\left(\frac{i}{N}, \frac{j}{N}\right)^{2H} + (1 - c_H)\,\tau_E\left(\frac{i}{N}, \frac{j}{N}\right)^2$
  end for
end for
for $i = 0$ to N **do**
  for $j = 1$ to $N - 1$ **do**
    $K_{per}(i, N + j) \leftarrow K_{per}(i, N - j)$
  end for
end for
for $j = 0$ to $N - 1$ **do**
  for $i = 1$ to $N - 1$ **do**
    $K_{per}(N + i, j) \leftarrow K_{per}(N - i, j)$
  end for
end for
for $i = 1$ to $N - 1$ **do**
  for $j = 1$ to $N - 1$ **do**
    $K_{per}(N + i, N + j) \leftarrow K_{per}(N - i, N - j)$
  end for
end for

Step 2. Compute the eigenvalues of the minimal symmetric circulant embedding matrix $\boldsymbol{S}$
$\tilde{\boldsymbol{s}} \leftarrow \mathrm{FFT2}(\boldsymbol{K_{per}})$

Step 3. Check the positivity of the eigenvalues
if $\min(\min(\Re(\tilde{s}))) \leq 0$ **then** break
end if

Step 4. Simulation of the periodic field $\boldsymbol{Y_{E,H}}$
$\varepsilon_1 \leftarrow$ Generate a $(2N, 2N)$-vector of i.i.d. $\mathcal{N}(0,1)$ random variables
$\varepsilon_2 \leftarrow$ Generate a $(2N, 2N)$-vector of i.i.d. $\mathcal{N}(0,1)$ random variables
$\boldsymbol{Y_{E,H}} \leftarrow \Re\Big(\mathrm{FFT2}((\boldsymbol{\varepsilon_1} + i\boldsymbol{\varepsilon_2}).*\sqrt{\tilde{\boldsymbol{s}}}\Big)/(2\boldsymbol{N})$

Step 5. Compute the two FBM $\boldsymbol{B_{a_1}}$ and $\boldsymbol{B_{a_2}}$
$B_{a_1} \leftarrow$ Apply Algorithm 1 with $a = a_1$
$B_{a_2} \leftarrow$ Apply Algorithm 1 with $a = a_2$

Step 6. Compute the OSGRF $\boldsymbol{X_{E,H}}$
Compute the size M of the simulation grid
for $i = 0$ to M **do**
  for $j = 0$ to M **do**
    $X_{E,H}(i,j) \leftarrow Y_{E,H}(i,j) - Y_{E,H}(0,0) + \sqrt{1 - c_H}(B_{a_1}(i) + B_{a_2}(j))$
  end for
end for

Output: $\boldsymbol{X_{E,H}}$ discretized OSGRF with parameter (E, H).

References

[1] P. Abry and F. Sellan. The wavelet-based synthesis for fractional Brownian motion proposed by F. Sellan and Y. Meyer: remarks and fast implementation. *Appl. Comput. Harmon. Anal.*, 3:377–383, 1996.

[2] D. Allard, R. Senoussi, and E. Porcu. Anisotropy models for spatial data. *Mathematical Geosciences*, 48, 2016.

[3] R. Askey. Radial characteristic functions, 1973. *Technical summary report #1262, University of Wisconsin, Madison Mathematics Research Center.*

[4] C. Baek, G. Didier, and V. Pipiras. On integral representations of operator fractional Brownian fields. *Statist. Probab. Lett.*, 92:190–198, 2014.

[5] C.L. Benhamou, S. Poupon, E. Lespessailles, S. Loiseau, R. Jennane, V. Siroux, W. Ohley, and L. Pothaud. Fractal analysis of radiographic trabecular bone texture and bone mineral density. *J. Bone Miner. Res.*, 16(4):697–703, 2001.

[6] D. Benson, M. M. Meerschaert, B. Bäumer, and H. P. Scheffler. Aquifer operator-scaling and the effect on solute mixing and dispersion. *Water Resour. Res.*, 42:1–18, 2006.

[7] H. Biermé, C.L. Benhamou, and F. Richard. Parametric estimation for Gaussian operator scaling random fields and anisotropy analysis of bone radiograph textures. In K. Pohl, editor, *Proc. of the International Conference on Medical Image Computing and Computer Assisted Intervention (MICCAI'09), Workshop on Probabilistic Model s for Medical Imaging*, pages 13–24, London, UK, september 2009.

[8] H. Biermé, A. Bonami, and León J. R. Central limit theorems and quadratic variations in terms of spectral density. *Electronic Journal of Probability*, 16(3):362–395, 2011.

[9] H. Biermé and C. Lacaux. Hölder regularity for operator scaling stable random fields. *Stoch. Proc. Appl.*, 119(7):2222–2248, 2009.

[10] H. Biermé, M. M. Meerschaert, and H. P. Scheffler. Operator scaling stable random fields. *Stoch. Proc. Appl.*, 117(3):312–332, 2007.

[11] H. Biermé, L. Moisan, and F. Richard. A turning-band method for the simulation of anisotropic fractional brownian fields. *J. Comput. Graph. Statist*, 24(3), 2015.

[12] A. Brouste, S. Lambert-Lacroix, and J. Istas. On fractional Gaussian random fields simulations. *Journal of Statistical Software*, 23(1):1–23, 2007.

[13] T. Candela, M. Bouchon, A. Brouste, D. Marsan, J. Schmittbuhl, and C. Voisin. Characterization of fault roughness at various scales: Implications of three-dimensional high resolution topography measurements. *Pure and Applied Geophysics*, 166((10-11)):1817–1851, 2009.

[14] G. Chan. An effective method for simulating Gaussian random fields. In *Proceedings of the statistical Computing section*, pages 133–138, `www.stat.uiowa.edu/~grchan/`, 1999. Amerir. Statist.

[15] J.F. Coeurjolly. Simulation and identification of the fractional brownian motion: a bibliographical and comparative study. *Journal of Statistical Software*, 5:153, 2000.

[16] P. F. Craigmile. Simulating a class of stationary Gaussian processes using the Davies-Harte algorithm, with application to long memory processes. *J. Time Ser. Anal.*, 24(5):505–511, 2003.

[17] S. Davies and P. Hall. Fractal analysis of surface roughness by using spatial data. *J. R. Stat. Soc. Ser. B*, 61:3–37, 1999.

[18] G. Didier, M. Meerschaert, and V. Pipiras. Exponents of operator self-similar random fields, 2016. *preprint.*

[19] C.R. Dietrich and G.N. Newsam. Fast and exact simulation of stationary gaussian processes through circulant embedding of the covariance matrix. *SIAM Journal of Scientific Computing*, 18(4):1088–1107, 1997.

[20] G. E. Fasshauer. *Meshfree approximation methods with MATLAB*, volume 6 of *Interdisciplinary Mathematical Sciences*. World Scientific Publishing Co. Pte. Ltd., Hackensack, NJ, 2007. With 1 CD-ROM (Windows, Macintosh and UNIX).

[21] W. Feller. *An introduction to probability theory and its applications. Vol. II.* Second edition. John Wiley & Sons, Inc., New York-London-Sydney, 1971.

[22] J. Istas. On fractional stable fields indexed by metric spaces. *Elect. Comm. in Probab.*, 11:242–251, 2006.

[23] A. N. Kolmogorov. Wienersche Spiralen und einige andere interessante Kurven in Hilbertsche Raum. *C. R. (Dokl.) Acad. Sci. URSS*, 26:115–118, 1940.

[24] J. Lévy Véhel. *Fractals in engineering: from theory to industrial applications*. Springer, New York, 1997.

[25] Y. Li, W. Wang, and Y. Xiao. Exact moduli of continuity for operator-scaling Gaussian random fields. *Bernoulli*, 21(2):930–956, 2015.

[26] R. Lopes and N. Betrouni. Fractal and multifractal analysis: a review. *Med Image Anal.*, 13(4):634–649, 2009.

[27] B. B. Mandelbrot and J. Van Ness. Fractional Brownian motion, fractional noises and applications. *SIAM Review*, 10:422–437, 1968.

[28] M. M. Meerschaert and H. P. Scheffler. *Limit distributions for sums of independent random vectors*. Wiley Series in Probability and Statistics: Probability and Statistics. John Wiley & Sons Inc., New York, 2001. Heavy tails in theory and practice.

[29] E. Pardo-Igúzquiza and M. Chica-Olmo. The Fourier integral method: an efficient spectral method for simulation of random fields. *Mathematical Geology*, 25(2):177–217, 1993.

[30] E. Perrin, R. Harba, R. Jennane, and I. Iribarren. Fast and exact synthesis for 1-D fractional Brownian motion a nd fractional gaussian noises. *IEEE Signal Processing Letters*, 9(11):382–384, 2002.

[31] G. Samorodnitsky and M. S. Taqqu. *Stable non-Gaussian random processes*. Stochastic Modeling. Chapman & Hall, New York, 1994. Stochastic models with infinite variance.
[32] I. J. Schoenberg. Metric spaces and completely monotone functions. *Ann. of Math. (2)*, 39(4):811–841, 1938.
[33] M. Shinozuka and C.-M. Jan. Digital simulation of random processes and its applications. *Journal of Sound and Vibration*, 25(1):111 – 128, 1972.
[34] M. L. Stein. Fast and exact simulation of fractional Brownian surfaces. *Journal of Computational and Graphical Statistics*, 11(3):587–599, 2002.
[35] W. Willinger, V. Paxson, and M. S. Taqqu. Self-similarity and heavy tails: Structural modeling of network traffic. In *A practical guide to heavy tails (Santa Barbara, CA, 1995)*, pages 27–53. Birkhäuser Boston, Boston, MA, 1998.
[36] A. Wood and G. Chan. Simulation of stationary Gaussian proceses on $[0,1]^d$. *Journal of Computational and Graphical Statistics*, 3(4):409–432, 1994.

Hermine Biermé, Laboratoire de Mathématiques et Applications, UMR-CNRS 7348, Université de Poitiers, Téléport 2-BP30179, Boulevard Marie et Pierre Curie, 86962 Chasseneuil, France.
E-mail address: hermine.bierme@math.univ-poitiers.fr

Céline Lacaux, Avignon Université, Laboratoire de Mathématiques d'Avignon (EA 2151), F-84018 Avignon; & Inria, BIGS, Villers-lès-Nancy, F-54600, France.
E-mail address: Celine.Lacaux@univ-avignon.fr